

Entanglement Islands and Infrared Anomalies in Schwarzschild Black Hole

D.S. Ageev, I.Ya. Aref'eva, A.I. Belokon, A.V. Ermakov, V.V. Pushkarev, and T.A. Rusalev

Steklov Mathematical Institute, Russian Academy of Sciences, Gubkin str. 8, 119991 Moscow, Russian Federation

E-mail: ageev@mi-ras.ru, arefeva@mi-ras.ru,
belokon.ai14@physics.msu.ru, ermakov@mi-ras.ru,
pushkarev@mi-ras.ru, rusalev@mi-ras.ru

ABSTRACT: In this paper, island formation for entangling regions of finite size in the asymptotically flat eternal Schwarzschild black hole is considered. We check the complementarity property of entanglement entropy which was implicitly assumed in previous studies for semi-infinite regions. This check reveals the emergence of infrared anomalies after regularization of a Cauchy surface. A naive infrared regularization based on “mirror symmetry” is considered and its failure is shown. We introduce an improved regularization that gives a correct limit agreed with the semi-infinite results from previous studies. As the time evolution goes, the endpoints of a finite region compatible with the improved regularization become separated by a timelike interval. We call this phenomenon the “Cauchy surface breaking”. Shortly before the Cauchy surface breaking, finite size configurations generate asymmetric entanglement islands in contrast to the semi-infinite case. Depending on the size of the finite regions, qualitatively new behaviour arises, such as discontinuous evolution of the entanglement entropy and the absence of island formation. Finally, we show that the island prescription does not help us to solve the information paradox for certain finite size regions.

Contents

| | | |
|----------|---|-----------|
| 1 | Introduction | 2 |
| 2 | Setup | 7 |
| 3 | Infrared regularization and complementarity property | 12 |
| 3.1 | Regularization of Cauchy surface | 13 |
| 3.2 | Semi-infinite interval | 15 |
| 3.3 | Finite interval | 16 |
| 3.4 | Multiple intervals | 17 |
| 3.5 | Asymmetric & Mirror-symmetric regularizations | 20 |
| 4 | Entropy for finite entangling regions | 21 |
| 4.1 | Asymmetric entangling regions | 24 |
| 4.2 | Mirror-symmetric entangling regions | 32 |
| 5 | Information loss paradox for finite entangling regions | 39 |
| 5.1 | Asymmetric entangling region | 42 |
| 5.2 | Mirror-symmetric entangling region | 43 |
| 6 | Conclusions & Future prospects | 47 |
| A | Explicit formulas for entanglement entropy with island | 49 |

1 Introduction

Hawking radiation is a mysterious and important phenomenon which provides a window to the world of quantum effects emerging in gravity [1, 2]. Having attracted the attention of physicists for years, it remains one of the main fingerprints of the quantum nature of black holes. Black holes, being thermodynamic systems, hint to us that we should study the entropy of the emitted radiation in order to understand their nature. Years ago, Page showed [3, 4] that a detailed comparison of the thermodynamic entropy of black holes and the entropy of their radiation leads to the fact that the entanglement entropy of this radiation exhibits an unlimited growth and, in the end, exceeds the Bekenstein-Hawking entropy of the black hole. This is in contradiction with the expected time dependence of the entanglement entropy visualized by the so-called Page curve, which should start to decrease after some characteristic time moment — the Page time. The descending part of the Page curve is difficult to interpret in a straightforward way, and recently a new mechanism called the “entanglement islands” [5–7] was introduced to explain the stoppage of the entanglement entropy growth. This mechanism arises when systems with dynamical gravitational degrees of freedom are considered, and the appearance of the entanglement islands is required for gravity to be consistent with the results of calculations performed using the replica trick. The conjecture of modifying the entanglement entropy in the presence of dynamical gravity has attracted a lot of attention in recent years [8–60, 63–74]. The entanglement islands has been studied in two-dimensional gravity setups [5, 12, 14, 15, 24, 25, 28, 34, 53], in boundary CFT models [13, 19, 41, 47, 58, 60–62, 65, 68, 74] and moving mirrors models [8–11, 32, 36, 37, 43, 50, 67].

In this paper, we study entanglement entropy and entanglement islands in the higher-dimensional Schwarzschild black hole following the setup proposed in [18]. In [18], the authors consider the s-wave approximation for fields defined on the background of the four-dimensional Schwarzschild black hole, effectively reducing the problem to a two-dimensional one while capturing the features of the higher-dimensional setup. This model explains how the unlimited growth of the entanglement entropy associated with semi-infinite regions “collecting” the Hawking radiation is stopped by emergence of the entanglement islands in the near-horizon zone of the Schwarzschild black hole. The variety of papers extending the results of [18] in the context of different models have appeared in recent years [22, 29, 30, 34, 35, 40, 42, 44, 46, 49, 51, 53, 54, 59, 63, 64, 66, 69–71].

In the framework of the s-wave approximation, we generalize the results of [18]

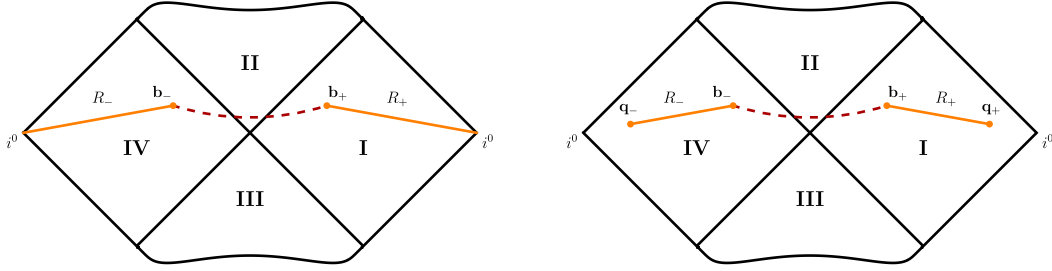


Figure 1: Left: Penrose diagram for the eternal Schwarzschild black hole with the *schematic* plots of the entangling region $R \equiv R_- \cup R_+$ (orange) and its complement $\bar{R} \equiv [\mathbf{b}_-, \mathbf{b}_+]$ (dashed red). **Right:** The same as in the left diagram but with the regularized semi-infinite entangling region R .

and consider entangling regions with a finite extent (instead of the semi-infinite ones studied in [18]). This problem, seemingly simple in its formulation, reveals curious features of the entanglement entropy in the two-sided Schwarzschild black hole. It is well known [25, 75] that for a pure bipartite quantum state, the entanglement entropies of each partition are equal to each other. This property is commonly used in the calculations of the entropy for semi-infinite regions. We explicitly check whether this “*complementarity property*” holds, i.e.

$$S(R) \stackrel{?}{=} S(\bar{R}), \quad (1.1)$$

(see Fig. 1 for the notation) and reveal, strictly speaking, its *violation*.

The complementarity property check involves the calculation of the entropy for semi-infinite regions, which can be done using the infrared (IR) regularization

$$S(R) = \lim_{\mathbf{q}_\pm \rightarrow i^0} S([\mathbf{q}_-, \mathbf{b}_-] \cup [\mathbf{b}_+, \mathbf{q}_+]), \quad (1.2)$$

see Fig. 1 for the configuration without islands. The regularized entangling region in the right wedge extends between the points \mathbf{b}_+ and \mathbf{q}_+ ; the left region starts at the point \mathbf{b}_- that is mirror-symmetric to \mathbf{b}_+ , i.e.

$$b_- = b_+, \quad t_{b_-} = -t_{b_+} + \frac{i\pi}{\kappa_h}, \quad (1.3)$$

where $\{b_\pm, t_{b_\pm}\}$ are Schwarzschild radial and time coordinates of the points \mathbf{b}_\pm .

In the same manner, one can also try to take the point \mathbf{q}_- as a mirror-symmetric one to \mathbf{q}_+

$$q_- = q_+, \quad t_{q_-} = -t_{q_+} + \frac{i\pi}{\kappa_h}. \quad (1.4)$$

We call this regularization scheme the “*mirror-symmetric*” (MS) regularization, since the regularized regions are mirror-symmetric¹ to each other, see Fig. 13. As we demonstrate, this treatment is *not* actually a regularization at all, since it does not possess the desired limit at spacelike infinity i^0 .

Our calculations show that the regularization should be such that Schwarzschild radial and time coordinates of the points \mathbf{q}_- and \mathbf{q}_+ are equal (up to the imaginary term $\frac{i\pi}{\kappa_h}$ for the time coordinate), i.e.

$$q_- = q_+, \quad t_{q_-} = t_{q_+} + \frac{i\pi}{\kappa_h}. \quad (1.5)$$

Only this regularization provides the complementarity property up to a violation term

$$S(R) = S(\overline{R}) + \frac{c}{3} \log \frac{2}{\kappa_h \varepsilon}. \quad (1.6)$$

We call this scheme the “*asymmetric*” (AS) regularization, since the regularized regions in the Penrose diagram are not symmetric in any sense, see Fig. 7. We interpret the second term on the RHS of (1.6) as an *anomaly* related to IR modes that violates the exact complementarity property. This type of regularization has a limit which coincides with the results of [18] (up to the anomaly term (1.6)), but contains a subtlety: the finite entangling region in the left wedge cannot be located on a constant time hypersurface and, moreover, if the radial coordinates are kept fixed, its endpoints become separated by a timelike interval during time evolution, thus the initial hypersurface is no longer spacelike. We refer to this phenomenon as the “*Cauchy surface breaking*”.

The same complementarity property problem arises for configurations with entanglement islands. Calculations for such configurations in works of different authors have assumed the equality between $S(R \cup I)$ and $S(\overline{R \cup I})$. We elaborate on this by defining

$$S(R \cup I) = \lim_{\mathbf{q}_\pm \rightarrow i^0} S([\mathbf{q}_-, \mathbf{b}_-] \cup [\mathbf{b}_+, \mathbf{q}_+] \cup I) \quad (1.7)$$

¹By mirror symmetry we mean the reflection about the vertical axis of symmetry of the Penrose diagram for the two-sided Schwarzschild black hole.

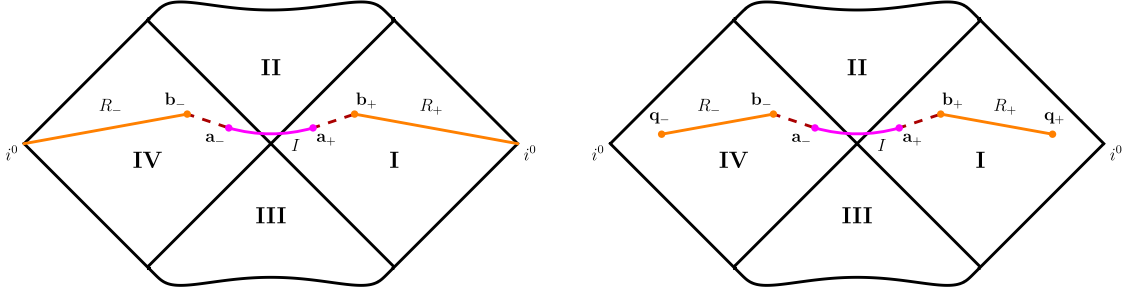


Figure 2: **Left:** Penrose diagram for the eternal Schwarzschild black hole with the *schematic* plots of the semi-infinite entangling region $R \equiv R_- \cup R_+$ (orange), its complement $\overline{R_- \cup R_+ \cup I} \equiv [b_-, a_-] \cup [a_+, b_+]$ (dashed red) and the entanglement island $I \equiv [a_-, a_+]$ (magenta). **Right:** the same as in the left diagram but with the regularized entangling region R .

(see Fig. 2 for the notation) and demonstrating that in the AS scheme, the following relation holds

$$S(R \cup I) = S(\overline{R \cup I}) + \frac{c}{3} \log \frac{2}{\kappa_h \varepsilon}, \quad (1.8)$$

i.e. once again, the same anomalous extra term (1.6) appears.

Regularization schemes (1.2) and (1.7) are related to the study of finite size effects in the behaviour of entanglement entropy. In accordance with the described regularization schemes, we consider two types of finite entangling regions with *fixed* radial coordinates of the points \mathbf{q}_\pm , and for both types we choose the points \mathbf{b}_\pm as in (1.3). Namely, the first and the second types of finite regions correspond to the choices of the points \mathbf{q}_\pm as in the mirror-symmetric (1.4) and asymmetric (1.5) regularizations. We call the finite regions of the first type *mirror-symmetric* (MS) (see Fig. 7), and of the second type — *asymmetric* (AS) (see Fig. 13). Note that the MS setup corresponds to finite configurations for the eternal black hole in two-dimensional AdS with flat reservoirs [48]. We should emphasize the difference between regularized and finite regions. We use the first ones to study the infrared behaviour of entanglement entropy and assume that the timelike coordinates are taken fixed while the radial ones go to spacelike infinity. In contrast, the radial coordinates of finite regions are fixed, and we study time evolution of their entropy. In particular, Cauchy surface breaking makes sense only for finite regions.

It is important to note that the finite size of entangling regions strongly affects the evolution picture, adding many qualitative features and influencing the behaviour of

the entanglement entropy. The dynamics of the latter for finite size configurations is very peculiar even beyond the island paradigm. Below we list our findings for finite size effects for the AS and MS entangling regions both with and without islands. They are as follows:

- **Finite entangling regions without islands:**

- The evolution of AS entangling regions suffers from a counterintuitive drawback — after some time, the entangling region in the left wedge is no longer spacelike, and we can say that the corresponding Cauchy surface breaks down. The time dependence of the entropy for these configurations corresponds to the semi-infinite case [18], with the only difference in the rapid decrease just before the Cauchy surface breaking.
- The time evolution of the entropy for MS entangling regions at relatively early times is given by a monotonic growth twice as fast as that of the entropy for the semi-infinite case [18]. The finite size effects lead to saturation of the entropy at late times when the fluxes of the radiation particles entering and leaving the region become equal.

- **Finite entangling regions with islands:**

- The existence of a new scale for AS entangling regions — the Cauchy surface breaking time — has important implications for entanglement islands as an effect inherent in late time evolution. It might happen that the breaking time occurs before the formation of the island, which makes the island formula of little use.
- At relatively early times, for AS entangling regions, a symmetric island configuration dominates. However, shortly before the Cauchy surface breaking, finite size effects come into play, making the entanglement island asymmetric in both spacelike and timelike directions. For sufficiently large regions at late times, the island saddle point dominates the matter contribution, thus stopping the growth of the entropy until the Cauchy surface breaking happens.
- For sufficiently large sizes of MS regions, entanglement islands exist only for a finite time due to the violation of extremization conditions for which they were found. Islands for MS regions are symmetric and lead to a monotonic growth of the entropy twice as slow as that for the same regions without islands. Since the lifetime of an island is finite, after its disappearance there

is a discontinuous transition to the no-island configuration. This leads to exceeding the allowed upper limit of the entropy, which we interpret as the information paradox for finite regions.

- For both AS and MS configurations, reducing the size of the entangling region can change the qualitative picture of the entropy evolution and forever make the entanglement entropy with an island subdominant. Moreover, for sufficiently small sizes, the island configuration is not generated at all.

Also, we discuss some universal modifications regarding the unitary evolution of the entropy of the Hawking radiation [3, 4] due to finite sizes of entangling regions in the context of the information paradox. For both AS and MS configurations, we show that in the limit $\mathbf{q}_{\pm} \rightarrow i^0$, the appropriate upper bound on the entropy [12, 18] is correctly reproduced. For sufficiently small regions, the introduction of islands is not required so that the entropy does not exceed this upper bound. However, for intermediate sizes of MS entangling regions, the entropy exceeds the upper bound for a finite time due to the discontinuous transition to the configuration without an island. Thus, one can assume that the introduction of an island for these regions does not lead to a satisfying resolution of the information paradox.

The paper is organized as follows. In Section 2, we present the setup for our further calculations. It contains a brief overview of the eternal Schwarzschild black hole geometry as well as a sketch of the results obtained in [18]. Section 3 is devoted to a discussion of the infrared regularizations and the complementarity property for semi-infinite entangling regions. In Section 4, we study the properties of the entanglement entropy for finite entangling regions. In Section 5, we discuss the information paradox for finite configurations. Section 6 gives a short summary and future perspectives. Appendix contains several long formulas.

2 Setup

Geometry

We start with the metric of the four-dimensional Schwarzschild black hole

$$ds^2 = -f(r)dt^2 + \frac{dr^2}{f(r)} + r^2 d\Omega_2^2, \quad f(r) = 1 - \frac{r_h}{r}, \quad (2.1)$$

where r_h corresponds to the horizon location, and $d\Omega_2^2$ is the spherical part of the metric. The surface gravity and the Hawking temperature of this black hole are defined as

$$\kappa_h = \frac{1}{2r_h}, \quad T = \frac{1}{4\pi r_h}. \quad (2.2)$$

Introducing Kruskal coordinates U and V corresponding to the right wedge of the eternal (two-sided) Schwarzschild black hole as²

$$\begin{aligned} U &= -\frac{1}{\kappa_h} e^{-\kappa_h u}, \quad u = t - r_*, \\ V &= \frac{1}{\kappa_h} e^{\kappa_h v}, \quad v = t + r_*, \end{aligned} \quad (2.3)$$

where u, v are retarded and advanced null coordinates, and $r_* = r_*(r)$ is the tortoise coordinate

$$r_*(r) = r + r_h \log\left(\frac{r - r_h}{r_h}\right), \quad (2.4)$$

the metric (2.1) of the Schwarzschild black hole can be rewritten in the form

$$ds^2 = -e^{2\rho(r)} dU dV + r^2 d\Omega^2, \quad (2.5)$$

where the conformal factor $\rho(r)$ is given by

$$e^{2\rho(r)} = \frac{r_h}{r} e^{-r/r_h}. \quad (2.6)$$

In what follows, we need a formula for the radial geodesic distance $d(\mathbf{x}, \mathbf{y})$ for the spherically symmetric two-dimensional part of the metric (2.5). If we consider (2.5) as the Weyl transformed version of the metric $ds^2 = -dU dV$ (neglecting the angular part) with the Weyl factor $e^{2\rho(r)}$, the square of the distance $d(\mathbf{x}, \mathbf{y})$ in the metric (2.5) can be derived as

$$d^2(\mathbf{x}, \mathbf{y}) = [U(\mathbf{x}) - U(\mathbf{y})] [V(\mathbf{y}) - V(\mathbf{x})] e^{\rho(\mathbf{x})} e^{\rho(\mathbf{y})}, \quad (2.7)$$

where by the bold letters we denote pairs of radial and time coordinates

$$\mathbf{x} = \{x, t_x\}. \quad (2.8)$$

²Sometimes we will refer to the global time defined as $U + V$.

In terms of (t, r) coordinates, one can explicitly rewrite (2.7) in the form

$$d^2(\mathbf{x}, \mathbf{y}) = \frac{2\sqrt{f(x)f(y)}}{\kappa_h^2} [\cosh \kappa_h(r_*(x) - r_*(y)) - \cosh \kappa_h(t_x - t_y)]. \quad (2.9)$$

The Kruskal coordinates covering the left wedge of the eternal Schwarzschild black hole are given by

$$\begin{aligned} U &= \frac{1}{\kappa_h} e^{-\kappa_h u}, \\ V &= -\frac{1}{\kappa_h} e^{\kappa_h v}. \end{aligned} \quad (2.10)$$

From the comparison of (2.3) and (2.10), we see that if we continue the timelike coordinate of the right wedge as $t \rightarrow t + \frac{i\pi}{\kappa_h}$, then we will find ourselves in the left wedge. This imaginary part implies the change of the Kruskal coordinates which corresponds to transition between the wedges.

We use the following notation for spacetime points

$$\begin{aligned} \mathbf{x}_+ &= \{x_+, t_{x_+}\}, \\ \mathbf{x}_- &= \left\{x_-, t_{x_-} + \frac{i\pi}{\kappa_h}\right\}, \end{aligned} \quad (2.11)$$

where the subscripts “+” and “−” denote the points in the right and the left wedges of the Penrose diagram for Schwarzschild spacetime, respectively.

Also, note there are two spacelike infinities i^0 in the Penrose diagram for the two-sided Schwarzschild black hole. For arbitrary spacetime points \mathbf{q}_\pm in the right and left wedges, we use a short-hand notation $\mathbf{q}_\pm \rightarrow i^0$ meaning the limits to different i^0 in the corresponding wedges. In this case, in the Schwarzschild patch (2.1), the radial coordinates of \mathbf{q}_\pm go to infinity: $q_\pm \rightarrow \infty$, while the timelike ones t_{q_\pm} are kept fixed.

Entanglement entropy

We study the entanglement entropy of massless conformal matter on the background (2.5). Generally speaking, the calculation of the entanglement entropy in a higher-dimensional curved spacetime is an extremely challenging problem, at least analytically. An important suggestion made in [18] is the consideration of the s-wave approximation of conformal four-dimensional matter, in which we neglect the spherical part of the metric (2.5) and effectively reduce the calculations to a two-dimensional problem. In this way, one

can consider the entanglement entropy of conformal matter in a two-dimensional metric and calculate it analytically. In this work, we will calculate the entanglement entropy of a system consisting of several finite intervals. In flat space, the entanglement entropy of a single interval between points x and y is given by

$$S = \frac{c}{3} \log \frac{|x - y|}{\varepsilon}, \quad (2.12)$$

while for a system of N intervals [76] we have

$$S = \frac{c}{3} \left(\sum_{i,j} \log \frac{|x_i - y_j|}{\varepsilon} - \sum_{i < j} \log \frac{|x_i - x_j|}{\varepsilon} - \sum_{i < j} \log \frac{|y_i - y_j|}{\varepsilon} \right), \quad (2.13)$$

where x_i and y_i are the left and right interval endpoints, and ε is the UV cutoff. The entanglement entropy in the curved spacetime (2.5) can be calculated using (2.9) and (2.13)

$$S_N = \frac{c}{3} \left(\sum_{i,j} \log \frac{d(\mathbf{x}_i, \mathbf{y}_j)}{\varepsilon} - \sum_{i < j} \log \frac{d(\mathbf{x}_i, \mathbf{x}_j)}{\varepsilon} - \sum_{i < j} \log \frac{d(\mathbf{y}_i, \mathbf{y}_j)}{\varepsilon} \right), \quad (2.14)$$

where \mathbf{x}_i and \mathbf{y}_i denote the left and right interval endpoints as in the flat space (2.13).

Entanglement islands in eternal Schwarzschild black hole

In the two-sided Schwarzschild black hole, we consider the Hartle-Hawking vacuum [77], for which the fluxes of outgoing and incoming radiation particles balance each other. The island mechanism can be schematically described as the appearance of an additional contribution from a region I to the entanglement entropy of an entangling region A . The region I is called the entanglement island and is located in spacetime according to certain rules [5, 7, 15, 78]. To calculate the entanglement entropy in such a system, one should consider the generalized entropy functional S_{gen} given by the so-called *island formula* [14, 15]

$$S_{\text{gen}}(A) = \min_{\partial I} \left\{ \text{ext}_{\partial I} \left[\frac{\text{Area}(\partial I)}{4G_N} + S_{\text{matter}}(A \cup I) \right] \right\}, \quad (2.15)$$

where ∂I denotes the boundary of the entanglement island I , G_N is Newton's constant and S_{matter} is the entanglement entropy of conformal matter. One has to extremize this functional over all possible island configurations and choose the minimal one after that.

In [18], authors considered two semi-infinite entangling regions R_+ and R_- (see Fig. 1), where R_+ is in the right wedge of the two-sided Schwarzschild black hole and extends from some point \mathbf{b}_+ ³

$$\mathbf{b}_+ = \{b, t_b\}, \quad (2.16)$$

to spacelike infinity i^0 . In turn, R_- is in the left wedge and extends from the point \mathbf{b}_-

$$\mathbf{b}_- = \left\{ b, -t_b + \frac{i\pi}{\kappa_h} \right\}, \quad (2.17)$$

to the corresponding spacelike infinity i^0 . The time coordinate in (2.17) is taken in accordance with the analytic continuation of the coordinates (2.1) to the left wedge.

As it was mentioned in Introduction, all previous papers on this topic have been based on the calculation of the entropy for finite complements of the entangling regions. In particular, given the region $R \equiv R_+ \cup R_-$ where the ‘‘Hawking quanta’’ are ‘‘collected’’ during the evolution, one can define the entanglement entropy of \bar{R} as

$$S(\bar{R}) \equiv S([\mathbf{b}_-, \mathbf{b}_+]). \quad (2.18)$$

The calculation of $S(\bar{R})$ is simple and leads to [18]

$$S(\bar{R}) = \frac{c}{6} \log \left[\frac{16r_h^2(b - r_h)}{\varepsilon^2 b} \cosh^2 \kappa_h t_b \right]. \quad (2.19)$$

In the limit when the boundaries of the entangling regions go to spacelike infinities i^0 (i.e. $b \rightarrow \infty$ at fixed t_b), this formula reduces to

$$\lim_{\mathbf{b}_\pm \rightarrow i^0} S(\bar{R}) = \frac{c}{3} \log \frac{2}{\varepsilon \kappa_h} + \frac{c}{3} \log \cosh \kappa_h t_b. \quad (2.20)$$

This is not what was expected, since in the limit of the vanishing region R , entangled particles of radiation are not collected, and the entanglement entropy should have been equal to zero. The first term on the RHS of (2.20) can be understood as the contribution to the entanglement entropy from the IR modes. This constant arises in further calculations and will be important for explaining of our results.

The entanglement entropy (2.19) at late times $t_b \gg r_h$ enters the unbounded linear

³The s-wave approximation works at $b \gg r_h$.

growth regime

$$S(\overline{R}) = \frac{c}{3} \kappa_h t_b, \quad (2.21)$$

that can be interpreted as a variation of the information paradox.

In [18], it was shown that with the introduction of entanglement islands this growth stops at some time moment, since the generalized entanglement entropy $S_{\text{gen}}(R)$ saturates. There is a symmetric island at late times with endpoints located in different wedges the horizon (see Fig. 2). These results were also obtained via the consideration of the complement of $R \cup I^4$

$$\min_{\partial I} \left\{ \text{ext}_{\partial I} \left[\frac{\text{Area}(\partial I)}{4G_N} + S_{\text{matter}}(\overline{R \cup I}) \right] \right\} \simeq \frac{2\pi r_h^2}{G_N} + \frac{c}{6} \left[\log \left(\frac{16r_h^3(b-r_h)^2}{\varepsilon^4 b} \right) + \frac{b-r_h}{r_h} \right]. \quad (2.22)$$

This entropy does not increase at late times as opposed to the late-time result without the island (2.21), and thus, according to the island formula (2.15), the configuration with the island is preferred.

For clarity of comparison with different types of finite regions in the following sections, we introduce the notation for the semi-infinite region $R_+ \cup R_-$ used above as

$$R_\infty \equiv R_+ \cup R_- = (i^0, \mathbf{b}_-] \cup [\mathbf{b}_+, i^0). \quad (2.23)$$

3 Infrared regularization and complementarity property

In this section, we are going to clarify the subtle points mentioned above. For this purpose, we study the entanglement entropy of the semi-infinite entangling region R_∞ . In studies exploring the model [18], the entropy of R_∞ is calculated under the assumption that it is equal to the entanglement entropy of the R_∞ complement (since they lie on the same Cauchy surface Σ which defines a pure quantum state). We call this statement the *complementarity property*. It is natural to ask how to calculate it directly representing R_∞ as the limit of some finite region (i.e. pass from Fig. 1 (right) to Fig. 1 (left)). At first sight, this might seem obvious, however, such a consideration contains subtleties which will give us further understanding of finite entangling regions and their edge effects. Let us list the results that will be important for further analysis:

- Regions R_+ and R_- should be defined on a *certain* Cauchy surface Σ . According to the complementarity property, the entanglement entropy of a pure state on R_∞ should be equal to the entanglement entropy of the R_∞ complement. We

⁴In [18], the entropy (2.22) is obtained in the leading order expansion in cG/r_h^2 .

check explicitly whether this property holds for the infinite region R_∞ defined as the limit of a finite one.

- Representation of an infinite entangling region as the limit of a finite one raises the issue of how to take this limit *correctly*, namely, how to pick the points \mathbf{q}_- and \mathbf{q}_+ in Fig. 1 before sending them to spacelike infinity i^0 . A naive way to choose finite entangling intervals is to take the points $\mathbf{q}_+ = \{q, t_q\}$ in the right wedge and $\mathbf{q}_- = \left\{q, -t_q + \frac{i\pi}{\kappa_h}\right\}$ in the left one (i.e. choose a radially-symmetric configuration at the same global time). We show that such a choice does not satisfy the complementarity property.
- As a result, we obtain two qualitatively different types of entangling regions — MS and AS. The MS configurations *fail* the complementarity test, while the AS ones do *not*. In the next section, we show that the AS regions also demonstrate interesting properties.
- We obtain that the complementarity property for regularized configurations holds *up to a constant* which depends on the black hole temperature and the UV cutoff of the entanglement entropy. This is exactly the constant defined in (2.20) which corresponds to the entanglement entropy associated with the IR modes. The presence of such an infrared anomalous term and the importance of the proper Cauchy surface regularization are reminiscent of the appearance of anomalies in quantum field theory due to regularization.

3.1 Regularization of Cauchy surface

Before considering different types of entangling regions, let us introduce the regularization of a Cauchy surface Σ which extends between spacelike infinities in the left and right wedges (see Fig. 3). To regularize Σ , we take a finite spacelike interval $\Sigma_{\text{reg}} = [\mathbf{q}_-, \mathbf{q}_+]$ with the coordinates of the endpoints

$$\begin{aligned}\mathbf{q}_- &= \left\{q_-, t_{q_-} + \frac{i\pi}{\kappa_h}\right\}, \\ \mathbf{q}_+ &= \{q_+, t_{q_+}\}.\end{aligned}\tag{3.1}$$

Then, the entanglement entropy of conformal matter on the regularized Cauchy surface Σ_{reg} is given by

$$S(\Sigma_{\text{reg}}) = \frac{c}{6} \log \frac{d^2(\mathbf{q}_-, \mathbf{q}_+)}{\varepsilon^2},\tag{3.2}$$

which is, in general, divergent. However, if we take $q_- = q_+ \equiv q$ and $t_{q_-} = t_{q_+} \equiv t_q$, we obtain the following expression

$$S(\Sigma_{\text{reg}}) = \frac{c}{6} \log \frac{4f(q)}{\varepsilon^2 \kappa_h^2}. \quad (3.3)$$

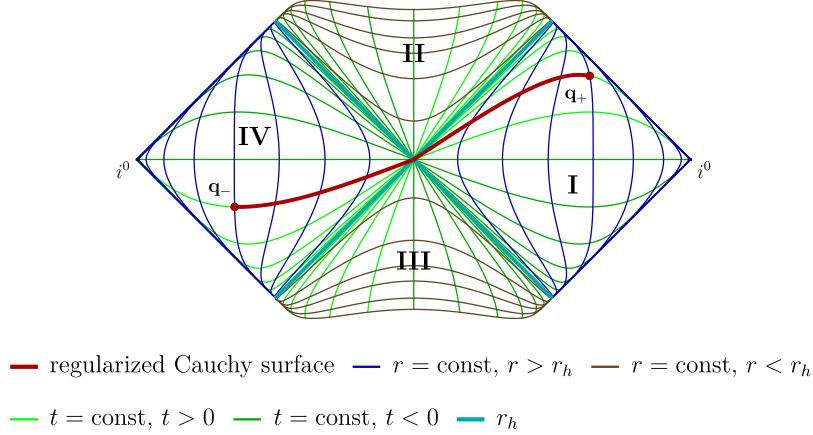


Figure 3: Penrose diagram for the eternal Schwarzschild black hole with the regularized Cauchy surface $\Sigma_{\text{reg}} \equiv [\mathbf{q}_-, \mathbf{q}_+]$, $\mathbf{q}_{\pm} \rightarrow i^0$.

The entanglement entropy of the whole Cauchy surface Σ is given by the limit $q \rightarrow \infty$ of (3.3) which we expect to be zero for a pure state. Taking into account that $f(q) \rightarrow 1$ as $q \rightarrow \infty$, we obtain

$$S(\Sigma) = \frac{c}{3} \log \frac{2}{\varepsilon \kappa_h}. \quad (3.4)$$

This is the same constant we have encountered in (2.20). As we have mentioned, this constant seems to be the contribution of the IR modes, and we should *renormalize* all the results by subtracting this constant from the final answers.

Now, let us check the complementarity property for certain configurations of entangling regions lying on the Cauchy surface Σ . For our future purposes, we consider:

- a semi-infinite interval (Fig. 4),
- a finite interval which lies arbitrarily in the left/right or both wedges of the Penrose diagram for Schwarzschild spacetime (Fig. 5),

- a union of two disjoint finite intervals one of which lies in the left wedge and the other in the right (Fig. 6).

3.2 Semi-infinite interval

First, let us check the complementarity property for a semi-infinite entangling region, spanning in the right wedge from the radial coordinate b to spatial infinity i^0 . Its complement extends from the spatial infinity in the left wedge to the the point with the same radial coordinate b . Our goal is to represent the semi-infinite entangling region and its complement as the limits of several finite regions (see Fig. 4). One can consider this procedure as a regularization of spacelike infinities. The regularized entangling region is located between the points \mathbf{b}_+ and \mathbf{q}_+ (dark red curve in Fig. 4), namely

$$\begin{aligned}\mathbf{b}_+ &= \{b, t_b\}, \\ \mathbf{q}_+ &= \{q_+, t_{q_+}\}.\end{aligned}\tag{3.5}$$

The regularized complement lies between the point \mathbf{q}_- in the left wedge and the point \mathbf{b}_+ in the right wedge (light red curve in Fig. 4), where \mathbf{q}_- is given by

$$\mathbf{q}_- = \left\{ q_-, t_{q_-} + \frac{i\pi}{\kappa_h} \right\}.\tag{3.6}$$

The calculation of the entanglement entropy $S([\mathbf{b}_+, \mathbf{q}_+])$ for this entangling region by use of (2.14) gives

$$S([\mathbf{b}_+, \mathbf{q}_+]) = \frac{c}{6} \log \left[\frac{2\sqrt{f(b)f(q)}}{\kappa_h^2 \varepsilon^2} \left(\cosh \kappa_h(r_*(b) - r_*(q_+)) - \cosh \kappa_h(t_b - t_{q_+}) \right) \right].$$

For the large q_+ limit, it reduces to

$$S([\mathbf{b}_+, \mathbf{q}_+]) \Big|_{q_+ \rightarrow \infty} = \frac{c}{12} \log q_+ + \frac{c}{6} \kappa_h (q_+ - b) - \frac{c}{6} \log \kappa_h^2 \varepsilon^2 \sqrt{b},\tag{3.7}$$

with the similar result for the entanglement entropy $S([\mathbf{q}_-, \mathbf{b}_+])$ of the complement

$$S([\mathbf{q}_-, \mathbf{b}_+]) \Big|_{q_- \rightarrow \infty} = \frac{c}{12} \log q_- + \frac{c}{6} \kappa_h (q_- - b) - \frac{c}{6} \log \kappa_h^2 \varepsilon^2 \sqrt{b}.\tag{3.8}$$

Thus, if the IR regulators \mathbf{q}_\pm are taken such that their radial coordinates are equal, $q_- = q_+ \equiv q$, the complementarity property is satisfied in the form

$$\lim_{\mathbf{q}_\pm \rightarrow i^0} \left(S([\mathbf{q}_-, \mathbf{b}_+]) - S([\mathbf{b}_+, \mathbf{q}_+]) \right) \Big|_{q_- = q_+} = 0.\tag{3.9}$$

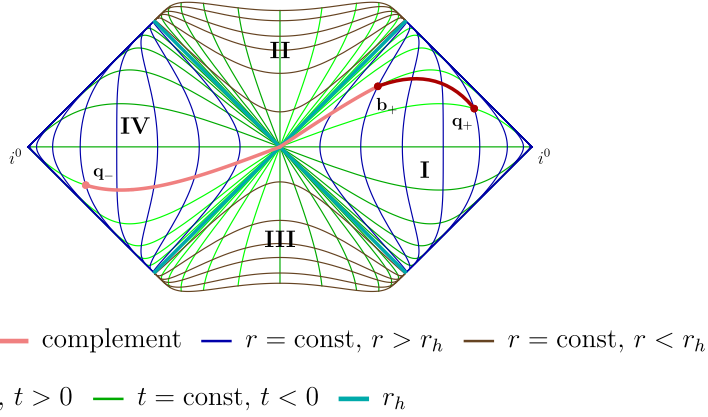


Figure 4: Penrose diagram for the eternal Schwarzschild black hole with the regularized semi-infinite configuration: the entangling region $[\mathbf{b}_+, \mathbf{q}_+]$ and its complement $[\mathbf{q}_-, \mathbf{b}_+]$, $\mathbf{q}_\pm \rightarrow i^0$.

Note that this result does *not* depend on the timelike coordinates of the regulators \mathbf{q}_\pm .

3.3 Finite interval

Now let us turn to the case when the entangling region R is given by a finite interval. We consider two different configurations. The first one is when the left endpoint \mathbf{b}_- is in the left wedge and the right endpoint \mathbf{y}_+ is in the right wedge. The second configuration corresponds to the endpoints both lying in the same wedge (in the right one for definiteness); in this case, we denote the left endpoint by \mathbf{b}_+ and the right one by \mathbf{y}_+ . The complement \bar{R} is, therefore, given by two semi-infinite intervals in each wedge extending to the corresponding spatial infinities i^0 . We proceed with a similar regularization of spacelike infinities in \bar{R} by introducing the points \mathbf{q}_- and \mathbf{q}_+ (see Fig. 5), as in the previous case. Explicitly, the coordinates of the mentioned points are defined as

$$\begin{aligned}
 \mathbf{y}_+ &= \{y, t_y\}, \\
 \mathbf{b}_+ &= \{b, t_b\}, \\
 \mathbf{b}_- &= \left\{ b, t_b + \frac{i\pi}{\kappa_h} \right\}, \\
 \mathbf{q}_+ &= \{q_+, t_{q_+}\}, \\
 \mathbf{q}_- &= \left\{ q_-, t_{q_-} + \frac{i\pi}{\kappa_h} \right\}.
 \end{aligned} \tag{3.10}$$

The entanglement entropy of the entangling region $R = [\mathbf{b}_\pm, \mathbf{y}_+]$ (i.e. for both choices of the left endpoint location) is given by

$$S(R) = \frac{c}{6} \log \left[\frac{2\sqrt{f(y)f(b)}}{\kappa_h^2 \varepsilon^2} \left(\cosh \kappa_h(r_*(b) - r_*(y)) \mp \cosh \kappa_h(t_b - t_y) \right) \right].$$

We compare this formula with the entanglement entropy of the regularized complement $\bar{R}_{\text{reg}} = [\mathbf{q}_-, \mathbf{b}_\pm] \cup [\mathbf{y}_+, \mathbf{q}_+]$

$$S(\bar{R}_{\text{reg}}) = \frac{c}{3} \log \frac{d(\mathbf{b}_\pm, \mathbf{y}_+)}{\varepsilon} + \frac{c}{3} \log \frac{d(\mathbf{q}_-, \mathbf{q}_+)}{\varepsilon} + \frac{c}{3} \log \left(\frac{d(\mathbf{y}_+, \mathbf{q}_+)d(\mathbf{b}_\pm, \mathbf{q}_-)}{d(\mathbf{y}_+, \mathbf{q}_-)d(\mathbf{b}_\pm, \mathbf{q}_+)} \right), \quad (3.11)$$

which in the limit $q_\pm \rightarrow \infty$, reduces to

$$S(\bar{R}_{\text{reg}})_{q_\pm \rightarrow \infty} = S(R) + \frac{c}{3} \log \frac{2}{\kappa_h \varepsilon} + F(q_+, q_-, t_{q_+}, t_{q_-}), \quad (3.12)$$

where

$$F(q_+, q_-, t_{q_+}, t_{q_-}) = \frac{c}{6} \log \left[\frac{\cosh \kappa_h(t_{q_+} - t_{q_-}) + \cosh \kappa_h(r_*(q_+) - r_*(q_-))}{2} \right]. \quad (3.13)$$

One can see that for a spatially symmetric regularization $q_+ = q_- \equiv q$ and for points \mathbf{q}_\pm lying on the same *time slice*, i.e. $t_{q_+} = t_{q_-} \equiv t_q$, we are left with

$$S(\bar{R}_{\text{reg}})_{q_\pm \rightarrow \infty} = S(R) + \frac{c}{3} \log \frac{2}{\kappa_h \varepsilon}, \quad (3.14)$$

which is exactly the complementarity property up to the anomaly (2.20). Also, the result does *not* depend on the wedge (left, right or both) in which the finite entangling region is located.

3.4 Multiple intervals

Having received some intuition, it is straightforward to consider two and more intervals. The simplest generalization is the configuration consisting of the union of two finite intervals $[\mathbf{a}_1, \mathbf{a}_2]$ (the left wedge) and $[\mathbf{a}_3, \mathbf{a}_4]$ (the right wedge) with arbitrary endpoint

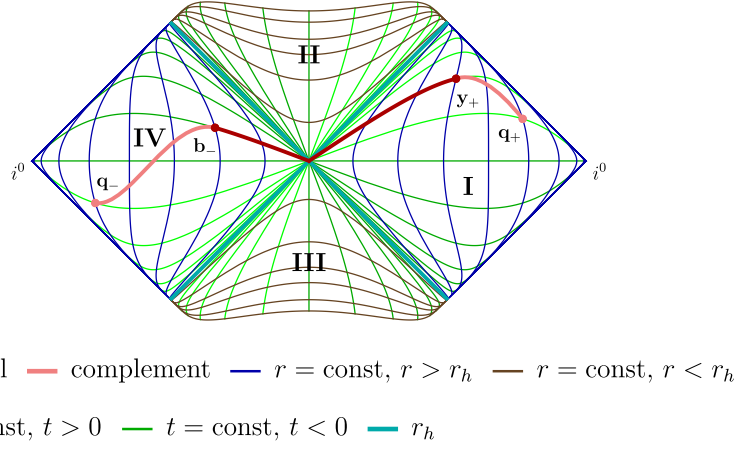


Figure 5: Penrose diagram for the eternal Schwarzschild black hole with the regularized finite interval configuration: the finite interval $[\mathbf{b}_-, \mathbf{y}_+]$ and its complement $[\mathbf{q}_-, \mathbf{b}_-] \cup [\mathbf{y}_+, \mathbf{q}_+]$, $\mathbf{q}_\pm \rightarrow i^0$.

coordinates (see Fig. 6)

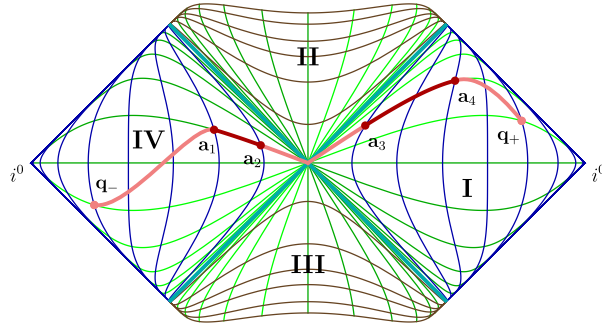
$$\begin{aligned}
\mathbf{a}_1 &= \left\{ a_1, t_{a_1} + \frac{i\pi}{\kappa_h} \right\}, \\
\mathbf{a}_2 &= \left\{ a_2, t_{a_2} + \frac{i\pi}{\kappa_h} \right\}, \\
\mathbf{a}_3 &= \{ a_3, t_{a_3} \}, \\
\mathbf{a}_4 &= \{ a_4, t_{a_4} \}.
\end{aligned} \tag{3.15}$$

Now, the entangling region R is defined as $R = [\mathbf{a}_1, \mathbf{a}_2] \cup [\mathbf{a}_3, \mathbf{a}_4]$ while the regularized complement $\bar{R}_{\text{reg}} = [\mathbf{q}_-, \mathbf{a}_1] \cup [\mathbf{a}_2, \mathbf{a}_3] \cup [\mathbf{a}_4, \mathbf{q}_+]$. The entanglement entropies of R and \bar{R}_{reg} are correspondingly given by

$$S(R) = \frac{c}{3} \log \left(\frac{d(\mathbf{a}_1, \mathbf{a}_2)d(\mathbf{a}_2, \mathbf{a}_3)d(\mathbf{a}_3, \mathbf{a}_4)d(\mathbf{a}_4, \mathbf{a}_1)}{\varepsilon^2 d(\mathbf{a}_1, \mathbf{a}_3)d(\mathbf{a}_2, \mathbf{a}_4)} \right) \tag{3.16}$$

and

$$\begin{aligned}
S(\bar{R}_{\text{reg}}) &= \frac{c}{3} \log \left(\frac{d(\mathbf{a}_1, \mathbf{a}_2)d(\mathbf{a}_2, \mathbf{a}_3)d(\mathbf{a}_3, \mathbf{a}_4)d(\mathbf{a}_4, \mathbf{a}_1)}{\varepsilon^2 d(\mathbf{a}_1, \mathbf{a}_3)d(\mathbf{a}_2, \mathbf{a}_4)} \right) + \frac{c}{3} \log \frac{d(\mathbf{q}_-, \mathbf{q}_+)}{\varepsilon} + \\
&+ \frac{c}{3} \log \left(\frac{d(\mathbf{a}_1, \mathbf{q}_-)d(\mathbf{a}_2, \mathbf{q}_+)d(\mathbf{a}_3, \mathbf{q}_-)d(\mathbf{a}_4, \mathbf{q}_+)}{d(\mathbf{a}_1, \mathbf{q}_+)d(\mathbf{a}_2, \mathbf{q}_-)d(\mathbf{a}_3, \mathbf{q}_+)d(\mathbf{a}_4, \mathbf{q}_-)} \right).
\end{aligned} \tag{3.17}$$



— interval — complement — $r = \text{const}, r > r_h$ — $r = \text{const}, r < r_h$
— $t = \text{const}, t > 0$ — $t = \text{const}, t < 0$ — r_h

Figure 6: Penrose diagram for the eternal Schwarzschild black hole with the regularized union of two finite intervals: the entangling region $[\mathbf{a}_1, \mathbf{a}_2] \cup [\mathbf{a}_3, \mathbf{a}_4]$ and its complement $[\mathbf{q}_-, \mathbf{a}_1] \cup [\mathbf{a}_2, \mathbf{a}_3] \cup [\mathbf{a}_4, \mathbf{q}_+]$, $\mathbf{q}_\pm \rightarrow i^0$.

After taking the large q_\pm , the latter takes the form

$$S(\bar{R}) \underset{q_\pm \rightarrow \infty}{=} S(R) + \frac{c}{3} \log \frac{2}{\kappa_h \varepsilon} + F(q_+, q_-, t_{q_+}, t_{q_-}). \quad (3.18)$$

Again, one can see that for a spatially symmetric regularization $q_- = q_+ \equiv q$ and the equal time slice choice $t_{q_-} = t_{q_+} \equiv t_q$, we obtain that the complementarity property is satisfied in the limit $\mathbf{q}_\pm \rightarrow i^0$ up to the constant (2.20).

It is straightforward to extend this calculation to the case when R consists of N intervals: $R = [\mathbf{a}_1, \mathbf{a}_2] \cup \dots \cup [\mathbf{a}_{N-1}, \mathbf{a}_N]$. Taking the IR regulators as in the previous cases, one can show that the entanglement entropy of the complement satisfies

$$S(\bar{R}_{\text{reg}}) = S(R) + \frac{c}{3} \log \frac{d(\mathbf{q}_-, \mathbf{q}_+)}{\varepsilon} + \frac{c}{3} \log \left(\frac{d(\mathbf{a}_1, \mathbf{q}_-) \dots d(\mathbf{a}_N, \mathbf{q}_+)}{d(\mathbf{a}_1, \mathbf{q}_+) \dots d(\mathbf{a}_N, \mathbf{q}_-)} \right). \quad (3.19)$$

In spatially symmetric equal time slice regularization, the third term on the RHS of (3.19) is identically zero, while the second term, which contains $d(\mathbf{q}_-, \mathbf{q}_+)$ and in general would be divergent, in our prescription, gives the constant contribution in the limit $\mathbf{q}_\pm \rightarrow i^0$ which is to be removed in the final formula.

3.5 Asymmetric & Mirror-symmetric regularizations

We have found that the representation of the entanglement entropy $S(R)$ of some entangling region R containing spacelike infinities in the left and right wedges as the limit of some finite regularized region has interesting properties. In such an entangling region, one should correctly regularize the semi-infinite intervals $[\mathbf{x}_+, i^0)$ and $(i^0, \mathbf{x}_-]$ by IR regulators \mathbf{q}_\pm such that the limits $\mathbf{q}_\pm \rightarrow i^0$ of $[\mathbf{q}_-, \mathbf{x}_-]$ and $[\mathbf{x}_+, \mathbf{q}_+]$ do not violate the complementarity property. To be more precise, these limits are well-defined and consistent with the complementarity property if

- The radial coordinates of the regularization points \mathbf{q}_\pm are taken equal: $q_- = q_+ \equiv q$. This is necessary for the limit $q \rightarrow \infty$ to exist.
- The regularization points \mathbf{q}_\pm lie on the same time slice $t_q = \text{const}$, i.e. the IR regulators are given by $\mathbf{q}_- = \left\{ q, t_q + \frac{i\pi}{\kappa_h} \right\}$ in the left wedge and $\mathbf{q}_+ = \{q, t_q\}$ in the right one.
- Final answers are renormalized by subtracting the constant $\frac{c}{3} \log \frac{2}{\varepsilon \kappa_h}$.

We combine these three conditions of regularizing spacelike infinities in the Schwarzschild two-sided geometry under the name “*asymmetric*” (AS) regularization.

Consider mirror-symmetric points \mathbf{q}_\pm , i.e. the conditions (1.4) are satisfied. We call such a choice the “*mirror-symmetric*” (MS) regularization. At first glance, this regularization seems more natural than the AS one. This is because, given the mirror symmetry (1.3) of the points \mathbf{b}_\pm , the regularized regions in the right and the left wedges are also mirror-symmetric, see Fig. 13. However, this regularization leads to a defect. Indeed, the function F (3.13) for MS regularization is

$$F_{\text{MS}}(q, q, t_q, -t_q) = \frac{c}{3} \log \cosh \kappa_h t_q. \quad (3.20)$$

Thus, the entropies of the entangling region and its complement, which includes spacelike infinities i^0 in both wedges, differ by a constant (2.20) and by a time-dependent function (3.20). As in AS regularization, the MS one uses the same prescription that the constant (2.20) is to be subtracted. Note that spacelike infinity i^0 does not correspond to a specific time — the points with arbitrary fixed times in the limit of infinite radial coordinates tend to i^0 . Therefore, the presence of the time dependence (3.20) in MS regularization leads to a significant discrepancy between the entropies of the region and its complement, as opposed to AS regularization.

For future purposes, let us introduce a short-hand notation which we call the “up-down” notation. We divide the interval endpoints \mathbf{x}_i into the “up” and “down” ones with respect to the horizontal line representing a hypersurface of the constant time $t = 0$ in the Penrose diagram for Schwarzschild spacetime. The “up” points are those which lie above this line (regardless of the wedge and the actual value of the time coordinate), and the “down” ones are those which lie below. Also note that in the right wedge, the Killing vector field ∂_t is directed from bottom to top, and in the left wedge — from top to bottom.

For clarity, let us write down the coordinates of arbitrary points $\mathbf{x}_\pm^{\text{up,down}}$ in the “up-down” notation

$$\begin{aligned} \mathbf{x}_+^{\text{up}} &= \{x, t_x\}, \\ \mathbf{x}_-^{\text{up}} &= \left\{x, -t_x + \frac{i\pi}{\kappa_h}\right\}, \\ \mathbf{x}_+^{\text{down}} &= \{x, -t_x\}, \\ \mathbf{x}_-^{\text{down}} &= \left\{x, t_x + \frac{i\pi}{\kappa_h}\right\}, \end{aligned} \tag{3.21}$$

where it is assumed that $t_x > 0$.

Now consider the entangling region R discussed in [18] and given by two semi-infinite intervals in each wedge which “collect” the Hawking radiation of the eternal Schwarzschild black hole. As we mentioned before, in [18] the entanglement entropy $S(R)$ was calculated with the use of the complementarity property: $S(R) = S(\bar{R})$. One can check explicitly that the calculation of the entanglement entropy $S(R)$ for the region R defined as the $\mathbf{q}_\pm \rightarrow i^0$ limit of the AS regularized configuration gives the same answer as in (2.19)

$$S(R) = \lim_{\mathbf{q}_\pm \rightarrow i^0} S([\mathbf{q}_-^{\text{down}}, \mathbf{b}_-^{\text{up}}] \cup [\mathbf{b}_+^{\text{up}}, \mathbf{q}_+^{\text{up}}]) = \frac{c}{6} \log \left(\frac{4f(b)}{\kappa_h^2} \cosh^2 \kappa_h t_b \right). \tag{3.22}$$

4 Entropy for finite entangling regions

Let us now turn to our main goal — the investigation of the entropy for finite regions affected by the presence of entanglement islands in the two-sided eternal Schwarzschild black hole. In Section 3, we made a statement that it is necessary to use AS regularization of spacelike infinities i^0 to be consistent with the complementarity property.

This statement specifies only an intermediate step in the calculation of the entropy for two *semi-infinite* regions in both wedges. At first sight, it seems that for *finite*

regions our previous results do not unambiguously specify the choice of their boundaries. However, as we show, the statement about AS regularization gives an intuition as to which finite regions are consistent with the results for the semi-infinite configuration obtained before [18]. In this section, we examine finite regions corresponding to both AS and MS schemes.

We consider the entropy of the following disjoint finite entangling region

$$R = [\mathbf{q}_-, \mathbf{b}_-] \cup [\mathbf{b}_+, \mathbf{q}_+], \quad (4.1)$$

where the first and the second finite parts are located in the left and the right wedges, respectively (see Fig. 7 and Fig. 13), and the coordinates of their boundaries are given by

$$\begin{aligned} \mathbf{b}_+ &= \{b_+, t_{b_+}\}, \\ \mathbf{q}_+ &= \{q_+, t_{q_+}\}, \\ \mathbf{b}_- &= \left\{b_-, t_{b_-} + \frac{i\pi}{\kappa_h}\right\}, \\ \mathbf{q}_- &= \left\{q_-, t_{q_-} + \frac{i\pi}{\kappa_h}\right\}. \end{aligned} \quad (4.2)$$

where, as in the previous section, $q_{\pm} > b_{\pm}$.

In [18], the boundaries of the semi-infinite regions \mathbf{b}_+ and \mathbf{b}_- have the time coordinates that are equal in absolute values but opposite in sign⁵, and the same radial coordinates, i.e.

$$t_{b_+} = -t_{b_-} \equiv t_b, \quad b_+ = b_- \equiv b. \quad (4.3)$$

This choice of the time coordinates makes the problem time-dependent in the case of semi-infinite intervals [12, 18]. Also, without loss of generality, we take \mathbf{q}_{\pm} radially symmetric

$$q_+ = q_- \equiv q, \quad (4.4)$$

and choose the time coordinates of the points \mathbf{b}_{\pm} , \mathbf{q}_{\pm} such that

$$|t_{q_+}| = |t_{q_-}| \equiv |t_b|, \quad (4.5)$$

with the following options for the choice of the relative sign:

⁵According to the notation introduced earlier, this means that \mathbf{b}_+ and \mathbf{b}_- are taken as the “up”-points.

- The first option is

$$t_{q_+} = t_{q_-}, \quad (4.6)$$

i.e. the points \mathbf{q}_+ and \mathbf{q}_- lie on the same time slice and correspond to AS regularization, see Fig. 7. Within the up-down notation, this corresponds to choosing the boundaries as $\mathbf{q}_-^{\text{down}}$ and \mathbf{q}_+^{up} ⁶

$$R_{\text{AS}} \equiv [\mathbf{q}_-^{\text{down}}, \mathbf{b}_-^{\text{up}}] \cup [\mathbf{b}_+^{\text{up}}, \mathbf{q}_+^{\text{up}}]. \quad (4.7)$$

We call this configuration the AS region. In Subsection 4.1, we will show that this is the case in which there is a correct limit for the entropy in the limit $\mathbf{q}_\pm \rightarrow i^0$. Also, notice that at some point, such a region becomes timelike which adds additional subtlety to the interpretation of this configuration.

- The second option is

$$t_{q_+} = -t_{q_-}, \quad (4.8)$$

see Fig. 13. This choice corresponds to MS regularization. Within the up-down notation, this corresponds to choosing the boundaries as \mathbf{q}_-^{up} and \mathbf{q}_+^{up}

$$R_{\text{MS}} \equiv [\mathbf{q}_-^{\text{up}}, \mathbf{b}_-^{\text{up}}] \cup [\mathbf{b}_+^{\text{up}}, \mathbf{q}_+^{\text{up}}]. \quad (4.9)$$

We denote this region as the MS region. In Subsection 4.2, we will show that in this case, the entropy in the limit $\mathbf{q}_\pm \rightarrow i^0$ does not correspond to the results for the semi-infinite setup [18].

So, after discussing the notation for entangling regions, it is appropriate to describe the island configuration which contributes to the generalized entanglement entropy. We restrict ourselves to the island given by a single interval and choose it similarly to [18]

$$I = [\mathbf{p}_-, \mathbf{a}_+], \quad (4.10)$$

with the boundary \mathbf{p}_- in the left wedge and the other boundary \mathbf{a}_+ in the right one (see Fig. 7 and Fig. 13), with the coordinates

$$\begin{aligned} \mathbf{a}_+ &= \{a, t_a\}, \\ \mathbf{p}_- &= \left\{ p, -t_p + \frac{i\pi}{\kappa_h} \right\}. \end{aligned} \quad (4.11)$$

⁶Since neither the left nor the right wedge is preferred, it does not really matter which one — right or left — has the “up”-point and which has the “down”-point. For clarity, we assume that the “down”-point is located in the left wedge.

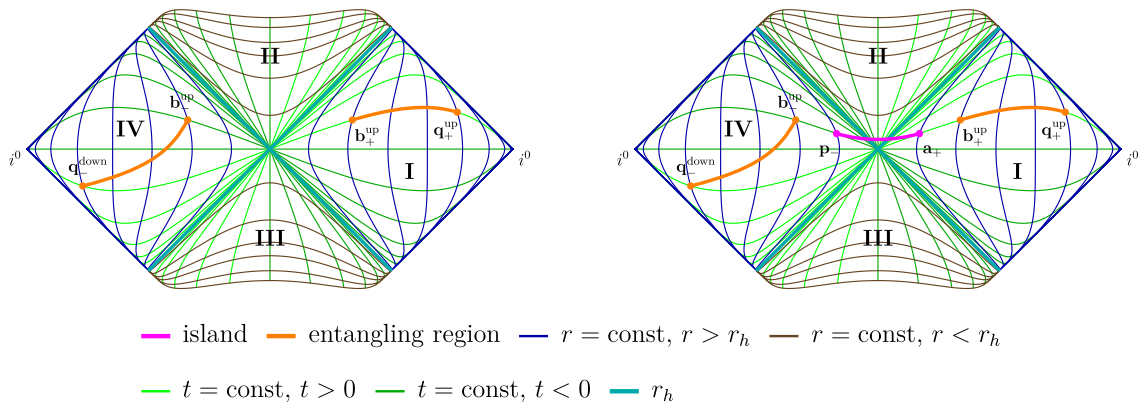


Figure 7: Left: Penrose diagram for the eternal Schwarzschild black hole with a finite AS entangling region $R_{\text{AS}} \equiv [\mathbf{q}_-^{\text{down}}, \mathbf{b}_+^{\text{up}}] \cup [\mathbf{b}_+^{\text{up}}, \mathbf{q}_+^{\text{up}}]$ (orange). **Right:** the same configuration with the island $I \equiv [\mathbf{p}_-, \mathbf{a}_+]$ (magenta).

In what follows, we show that for the entangling region R_{MS} , the island configuration reads: $a = p$, $t_a = t_p$, and that this is not the case for R_{AS} . We expect that at least for one of the types of entangling regions, the results for the semi-infinite case are reproduced for large sizes. We investigate the island configuration for different sizes of entangling regions, i.e. for different b and q .

Taking for our analysis the analytical formula for the entropy before extremization, expression in square brackets in (2.15), we find numerically the solutions (a, t_a, p, t_p) to the extremization equations for different sizes of finite entangling regions and investigate time dependence of the entropy with the island⁷. As discussed in Section 2, for semi-infinite intervals one can find a non-trivial symmetric island configuration at late times with endpoints located in different wedges in the near-horizon zone. We extend these results to the case when the entangling region is finite and, for generality, consider both R_{AS} and R_{MS} .

4.1 Asymmetric entangling regions

First, we consider the entanglement entropy for the finite entangling region R_{AS} (4.7) that corresponds to AS regularization (see Fig. 7). We show that for this region, the results for the semi-infinite one [18] are reproduced in the $\mathbf{q}_\pm \rightarrow i^0$ limit. We

⁷Our analytical analysis is somehow naive because we investigate the entropy for configurations with islands before extremization and not the extremization equations themselves. However, numerical analysis shows that this naive approach gives correct results.

also demonstrate that due to the non-constant time location of the region R_{AS} , such phenomena as Cauchy surface breaking and an asymmetric island arise.

No island

The entanglement entropy for R_{AS} (4.7) is given by (2.14)

$$S(R_{\text{AS}}) = \frac{c}{3} \log \left(\frac{d(\mathbf{b}_+^{\text{up}}, \mathbf{b}_-^{\text{up}}) d(\mathbf{q}_-^{\text{down}}, \mathbf{b}_-^{\text{up}}) d(\mathbf{b}_+^{\text{up}}, \mathbf{q}_+^{\text{up}}) d(\mathbf{q}_-^{\text{down}}, \mathbf{q}_+^{\text{up}})}{d(\mathbf{b}_-^{\text{up}}, \mathbf{q}_+^{\text{up}}) d(\mathbf{q}_-^{\text{down}}, \mathbf{b}_+^{\text{up}})} \right), \quad (4.12)$$

which, after substitution of coordinates, can be written down explicitly as

$$S(R_{\text{SE}}) = \frac{c}{6} \log \left(\frac{16f(b)f(q) \cosh^2 \kappa_h t_b}{\kappa_h^4 \varepsilon^4} \right) + \frac{c}{6} \log \left[\frac{(\cosh \kappa_h (r_*(q) - r_*(b)) - \cosh 2\kappa_h t_b) (\cosh \kappa_h (r_*(q) - r_*(b)) - 1)}{(\cosh \kappa_h (r_*(q) - r_*(b)) + \cosh 2\kappa_h t_b) (\cosh \kappa_h (r_*(q) - r_*(b)) + 1)} \right]. \quad (4.13)$$

The limit $\mathbf{q}_\pm \rightarrow i^0$ in AS regularization gives the same answer for the entropy (4.13) as in (2.19)

$$\lim_{\mathbf{q}_\pm \rightarrow i^0} S(R_{\text{AS}}) = S(R_\infty). \quad (4.14)$$

For the finite region R_{AS} , one inevitably meets a problem that there is an *upper bound* on time t_b . This happens because during time evolution, the interval at some point becomes timelike. Indeed, consider the square of the distance between $\mathbf{q}_-^{\text{down}}$ and \mathbf{b}_-^{up}

$$d^2(\mathbf{q}_-^{\text{down}}, \mathbf{b}_-^{\text{up}}) \propto \cosh \kappa_h (r_*(q) - r_*(b)) - \cosh 2\kappa_h t_b. \quad (4.15)$$

As we see, it gets negative after the time t_b^{break} that is given by

$$t_b^{\text{break}} = \frac{r_*(q) - r_*(b)}{2}. \quad (4.16)$$

As time evolution goes, the point \mathbf{b}_-^{up} moves forward in time along the flow of the Killing vector ∂_t , and the point $\mathbf{q}_-^{\text{down}}$ moves backward (see Fig. 7), such that at $t_b > t_b^{\text{break}}$ the interval between them is precisely timelike. This means that the Cauchy surface, which is a spacelike hypersurface spanned between spacelike infinities i^0 and includes the points $\mathbf{b}_\pm, \mathbf{q}_\pm$, at time t_b^{break} ceases to be such. We conclude that at $t_b > t_b^{\text{break}}$, the problem becomes ill-defined since there is no longer a Cauchy surface on which a pure quantum state is defined. Also, from (4.16) it follows that a larger finite region R_{AS} corresponds to a larger t_b^{break} . For an infinite region, which corresponds to $q \rightarrow \infty$ (and $r_*(q) \rightarrow \infty$), this time is infinite: $t_b^{\text{break}} \rightarrow \infty$, and the problem of Cauchy surface

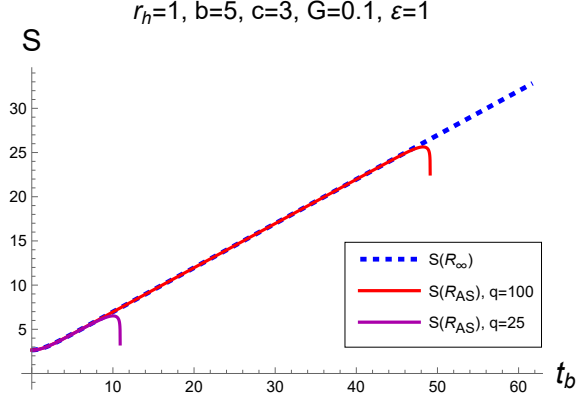


Figure 8: No-island entropy evolution for the finite entangling region R_{AS} with $q = 25$ (darker magenta), $q = 100$ (red) and for the semi-infinite one R_∞ (blue dashed). For all cases we take $b = 5$. Note that the curves have the same slope before the breaking time t_b^{break} (4.16) (different for each q).

breaking disappears.

For intermediate times $r_h \ll t_b \ll t_b^{\text{break}}$, the entanglement entropy for R_{AS} given by (4.13) grows linearly

$$S(R_{AS}) \simeq \frac{c}{3} \kappa_h t_b. \quad (4.17)$$

The entanglement entropy for a finite AS region follows the same curve as for the semi-infinite one, without strong dependence on b and q . Only just before the breaking time t_b^{break} (4.16), the entropy decreases and after t_b^{break} , it is not well-defined (see Fig. 8).

Inclusion of island

Now let us turn to the island configuration for R_{AS} . For the semi-infinite entangling region [18], the island is symmetric while for the finite region R_{AS} , the interval $[\mathbf{b}_+^{\text{up}}, \mathbf{q}_+^{\text{up}}]$ in the right wedge is not symmetric⁸ with respect to the interval $[\mathbf{q}_-^{\text{down}}, \mathbf{b}_-^{\text{up}}]$ in the left one, see Fig. 7. This makes the problem more complicated, meaning that the coordinates of the island boundaries \mathbf{a}_+ and \mathbf{p}_- in different wedges are not supposed to depend on each other.

According to the island formula (2.15), the entropy for a non-trivial island configuration before the extremization procedure has the form

$$S_I(R_{AS}) = \frac{\text{Area}(\partial I)}{4G} + S_{\text{matter}}(R_{AS} \cup I). \quad (4.18)$$

⁸Again, by “symmetric configurations” we mean those whose parts are mirrored with respect to the vertical axis of symmetry of the Penrose diagram for the eternal Schwarzschild black hole.

The area of the island boundary is

$$\frac{\text{Area}(\partial I)}{4G} = \frac{\pi(a^2 + p^2)}{G}. \quad (4.19)$$

The second term on the RHS of (4.18) is the entanglement entropy of the union of the entangling region (4.7) and the island (4.10). It is given by

$$S_{\text{matter}}(R_{\text{AS}} \cup I) = \mathcal{Y}(a, p, b, q, t_a, t_p, t_b), \quad (4.20)$$

where \mathcal{Y} is the function of the time and radial coordinates of $R_{\text{AS}} \cup I$. Due to its cumbersome form, the explicit expression for \mathcal{Y} (A.2) is presented in Appendix A.

The limit $\mathbf{q}_{\pm} \rightarrow i^0$ of the entropy before extremization (4.18) in AS regularization scheme coincides with the results for the semi-infinite regions [18]

$$\lim_{\mathbf{q}_{\pm} \rightarrow i^0} S_I(R_{\text{AS}}) = S_I(R_{\infty}). \quad (4.21)$$

According to the island prescription (2.15), the entanglement entropy (4.18) is to be extremized with respect to the parameters (a, t_a, p, t_p) ⁹.

For a moment, let us discuss the formula (4.20) to obtain some intuition about different regimes of the island dynamics. Consider the term which is not symmetric under the exchange $a \leftrightarrow p, t_a \leftrightarrow t_p$

$$\frac{c}{6} \log \left[\frac{(\cosh \kappa_h(r_*(q) - r_*(a)) + \cosh \kappa_h(t_a - t_b)) (\cosh \kappa_h(r_*(q) - r_*(p)) + \cosh \kappa_h(t_p + t_b))}{(\cosh \kappa_h(r_*(q) - r_*(a)) - \cosh \kappa_h(t_a - t_b)) (\cosh \kappa_h(r_*(q) - r_*(p)) - \cosh \kappa_h(t_p + t_b))} \right]. \quad (4.22)$$

This term does not significantly contributes to the entanglement entropy at relatively early times, by which we mean

$$\cosh \kappa_h(r_*(q) - r_*(p)) \gg \cosh \kappa_h(t_p + t_b), \quad (4.23)$$

$$\cosh \kappa_h(r_*(q) - r_*(a)) \gg \cosh \kappa_h(t_a - t_b). \quad (4.24)$$

Thus, it is reasonable to assume a symmetric island configuration $a \simeq p, t_a \simeq t_p$. Under this condition, the extremization procedure for (4.18) actually does not differ from that

⁹As we mentioned in Section 4.1, for the no-island configuration (4.7) there is an upper bound on time (4.16), since at $t_b > t_b^{\text{break}}$, the points $\mathbf{b}_{-}^{\text{up}}$ and $\mathbf{q}_{-}^{\text{down}}$ are timelike-separated. With the inclusion of the island, it might be possible that a similar condition arises for the boundaries of the region R_{AS} and the island. Numerical analysis shows that this happens after t_b^{break} .

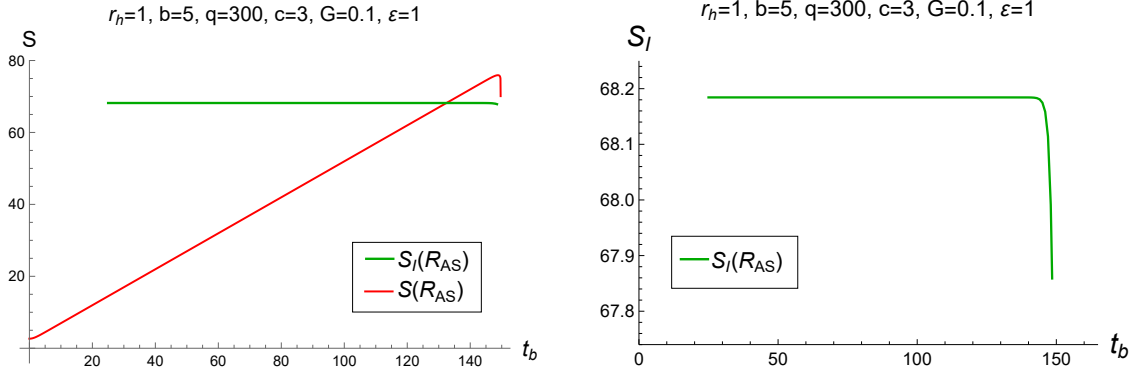


Figure 9: Left: entanglement entropy evolution for the region R_{AS} (red), and for the same region with the island (green). **Right:** entanglement entropy $S_I(R_{AS})$ in a different scale. For both plots, $b = 5$ and $q = 300$. Notice the abrupt decrease near $t_b^{\text{break}} = 150$ (4.16) caused by the finite size of the configuration.

for the semi-infinite region, where at late times

$$\cosh \kappa_h(t_a + t_b) \gg \cosh \kappa_h(r_*(a) - r_*(b)), \quad (4.25)$$

one can obtain an analytical estimate of the island location.

In fact, the condition (4.25) determines the moment, denoted by t_b^{isl} , when the island configuration appears. Due to the existence of the upper bound on time t_b^{break} (4.16), there is an additional restriction on the ratio between t_b^{isl} and t_b^{break} — the interval cannot become timelike faster than the island appears. If the condition

$$t_b^{\text{isl}} \ll t_b^{\text{break}} \quad (4.26)$$

is satisfied, which is expected for sufficiently large sizes of AS finite regions, then the “early time” extremization gives the same solution as in [18]

$$\begin{aligned} t_a &= t_p = t_b, \\ a &= p, \\ a - r_h &\ll r_h. \end{aligned} \quad (4.27)$$

For the island configuration (4.27), long before the breaking time t_b^{break} , one can write

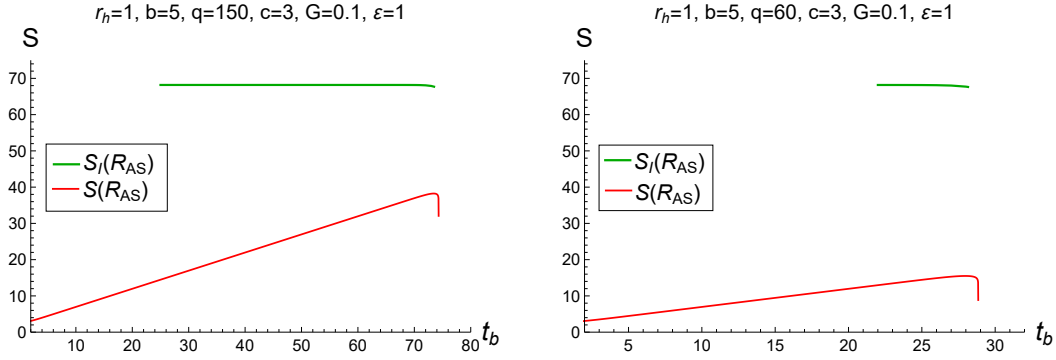


Figure 10: **Left:** entanglement entropy evolution for the region R_{AS} with $q = 150$ (red), and for the same region with the island I (green). **Right:** the same, but with $q = 60$. For both cases, we take $b = 5$. Notice that the entropy with the island I is not preferred by (2.15) over that for the no-island configuration.

down the analytical expression for the extremized entropy with the island¹⁰

$$\begin{aligned}
S_I(R_{AS}) \simeq & \frac{2\pi r_h^2}{G} + \frac{c}{6} \left[\log \left(\frac{16r_h^3(b-r_h)^2}{b\epsilon^4} \right) + \frac{b-r_h}{r_h} \right] \\
& + \frac{c}{6} \log \frac{4f(q)}{\kappa_h^2 \epsilon^2} - \frac{c}{3} e^{2\kappa_h t_b - \kappa_h(r_*(q) - r_*(b))},
\end{aligned} \tag{4.28}$$

see Appendix A for the details of derivation of (4.28). The entropy (4.28) differs from that with an island (2.22) for the semi-infinite regions R_∞ by the last two terms related to finite size effects. In the limit $\mathbf{q}_\pm \rightarrow i^0$ of (4.28) in AS regularization, the entropy (2.22) is reproduced.

By numerical extremization of the island configuration, we confirm that at late times, the term (4.22) gets significant, such that shortly before the breaking time t_b^{break} , the extremization over a and t_a does not change much, but the extremization over p and t_p introduces a *non-symmetric* island configuration. In this case, the formula (4.28) for the entropy is no longer valid.

We have found the extremum of the generalized entropy functional (2.15) numerically and determined the finite size effects inherent to entanglement evolution of AS regions:

- Time dependence of the entanglement entropy affected by the island is depicted in Fig. 9 and 10. In Fig. 9, we present the evolution of the entropy for a large

¹⁰The formula (4.28) is valid at $t_b \ll t_b^{\text{break}}$. Therefore, $e^{\kappa_h(r_*(q) - r_*(b))} \gg e^{2\kappa_h t_b}$, and the exponential growth in time in (4.28) is significantly suppressed.

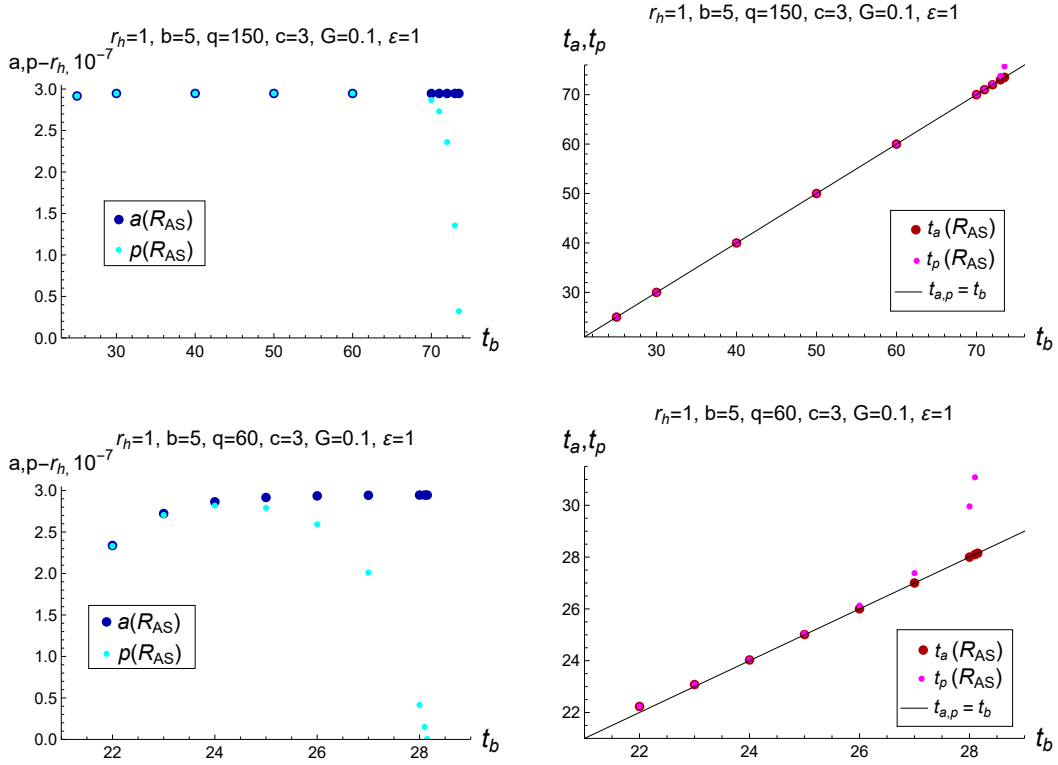


Figure 11: Left: evolution of the radial island coordinates a (darker blue), p (cyan) corresponding to the finite size entangling region R_{AS} . **Right:** evolution of the time island coordinates t_a (darker red), t_p (magenta) corresponding to the same region. Notice that near the breaking time t_b^{break} (4.16) one can observe spatial asymmetry $a \neq p$ and time assymetry $t_a \neq t_p$.

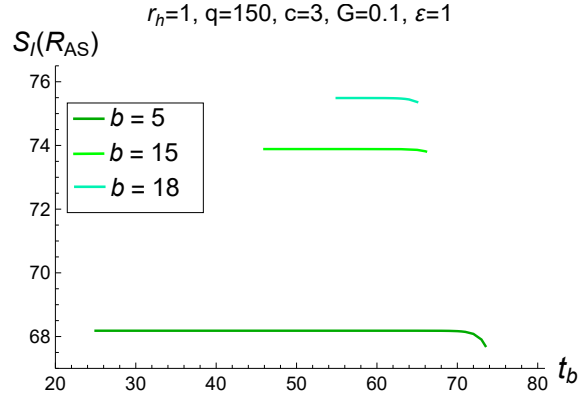


Figure 12: Time evolution of the entanglement entropy for $R_{AS} \cup I$ with $b = 5$ (green), $b = 15$ (light green) and $b = 18$ (cyan). For all cases, we take $q = 150$.

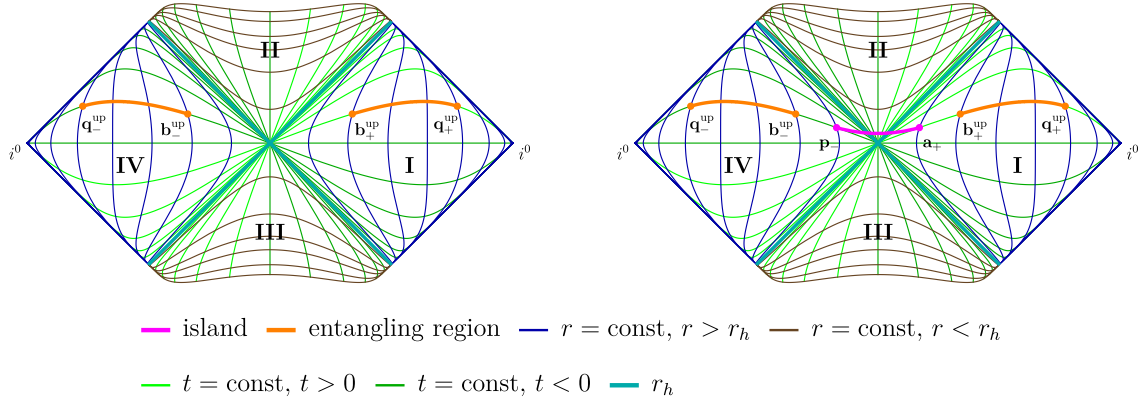


Figure 13: **Left:** Penrose diagram for the eternal Schwarzschild black hole with the mirror-symmetric entangling region $R_{\text{MS}} \equiv [\mathbf{q}_-^{\text{up}}, \mathbf{b}_-^{\text{up}}] \cup [\mathbf{b}_+^{\text{up}}, \mathbf{q}_+^{\text{up}}]$. **Right:** the same configuration with the island $I \equiv [\mathbf{p}_-, \mathbf{a}_+]$.

but still finite entangling region. Initially, the entropy follows the “canonical” picture of the linear growth (red curve). Then, the transition to the dominant island configuration happens (green curve), and the entropy, remaining approximately constant (4.28) for some time, slightly decreases just before the breaking time t_b^{break} .

- For a smaller region (Fig. 10), the picture is qualitatively different. Again, at early and intermediate times, the entropy grows approximately like in the semi-infinite case [18]. However, the island contribution is never dominant, so the whole evolution is determined only by the entanglement entropy of the matter in the entangling region.
- At early times (if the island appears), we observe the mirror-symmetric regime (4.27), while shortly before the breaking time t_b^{break} , we see significant deviation from the space and time symmetry between the island boundaries lying in different wedges (see Fig. 11).
- When reducing the size of the entangling region R_{AS} , the lifetime of the island decreases. At fixed b and decreasing q , t_b^{isl} does not change significantly, while t_b^{break} decreases (see Fig. 9 and 10). At fixed q and increasing b , t_b^{isl} increases, and t_b^{break} decreases (see Fig. 12). For sufficiently large b and small q , an island does not appear at all.

4.2 Mirror-symmetric entangling regions

As we saw in the previous section, one has to consider finite regions R_{AS} to reproduce the results obtained in [18]. In this section, we consider the entanglement entropy of Hawking radiation using the island formula (2.15) for finite MS entangling regions R_{MS} (4.9) (see Fig. 13). We show that for such regions, the results for the semi-infinite ones [18] are not reproduced in the $\mathbf{q}_{\pm} \rightarrow i^0$ limit.

As we mentioned in Subsection 3.5, the region R_{MS} seems more natural than R_{AS} because its parts in the right and left wedges are mirror-symmetric (see Fig. 13). Therefore, the boundaries of the parts of the entangling region R_{MS} located in the same wedge can have the same Schwarzschild time coordinates. From a three-dimensional purely spatial point of view, one can imagine each part of R_{MS} as a domain between two concentric spheres with radii b and q . Outgoing Hawking modes pass through this domain in finite time and then escape to infinity.

Even though R_{MS} does not give the correct limit $\mathbf{q}_{\pm} \rightarrow i^0$, it can still be used to test the island formula (2.15), capturing the interplay between gravity and entanglement and being well understood from the “naive” and “physical” points of view.

No island

Let us consider the entanglement entropy of Hawking radiation collected in the finite region (4.9) depicted in Fig. 13

$$S(R_{\text{MS}}) = \frac{c}{6} \log \left(\frac{16f(b)f(q)}{\kappa_h^4 \varepsilon^4} \cosh^4 \kappa_h t_b \right) + \frac{c}{3} \log \left(\frac{\cosh \kappa_h (r_*(q) - r_*(b)) - 1}{\cosh \kappa_h (r_*(q) - r_*(b)) + \cosh 2\kappa_h t_b} \right). \quad (4.29)$$

One can see that in the limit $\mathbf{q}_{\pm} \rightarrow i^0$, the entropy (4.29) does not reproduce the answer (2.19). Indeed, due to (3.20)

$$\lim_{\mathbf{q}_{\pm} \rightarrow i^0} S(R_{\text{MS}}) = S(R_{\infty}) + \frac{c}{3} \log \cosh \kappa_h t_b. \quad (4.30)$$

At relatively early times, when

$$\cosh 2\kappa_h t_b \ll \cosh \kappa_h (r_*(q) - r_*(b)), \quad (4.31)$$

but $t_b \gg r_h$, the entropy (4.29) without islands increases monotonically as

$$S(R_{\text{MS}}) \simeq \frac{2c}{3} \kappa_h t_b. \quad (4.32)$$

We observe the linear growth twice as fast as for R_∞ and R_{AS} , see (2.21) and (4.17). This behaviour and the incorrect limit (4.30) arise due to the fact that the distance between the boundaries \mathbf{q}_- and \mathbf{q}_+ is now time-dependent since they lie on different time slices. Also, provided that $t_b = t_q$, this time dependence is exactly the same as that of the distance between \mathbf{b}_- and \mathbf{b}_+ which doubles the coefficient in (4.32).

At late times, when the inequality (4.31) holds in the opposite direction, the entropy without islands (4.29) saturates at the value independent of time

$$S(R_{\text{MS}}) \simeq \frac{c}{6} \log \left(\frac{f(b)f(q)}{\kappa_h^4 \varepsilon^4} \right) + \frac{c}{3} \log (\cosh \kappa_h (r_*(q) - r_*(b)) - 1). \quad (4.33)$$

If $q \gg b$, we get from (4.33)

$$S(R_{\text{MS}}) \simeq \frac{c}{3} \kappa_h (r_*(q) - r_*(b)). \quad (4.34)$$

This saturation can be interpreted as follows. As soon as the “first”¹¹ particle of radiation from the black hole reaches the sphere of smaller radius b , the entropy starts to increase monotonically because more and more particles reach the domain between the spheres with radii b and q . As this particle reaches the sphere of radius q , the fluxes of incoming and outgoing particles become equal. Therefore, the entropy without islands saturates at some finite value.

Unlike the configuration R_{AS} (4.7), which has an upper bound on time, the configuration R_{MS} (4.9) does not have such a problem since the points $\mathbf{b}_\pm, \mathbf{q}_\pm$ in both right and left wedges move forward in time. The comparison of the entropies for R_∞ (2.19) and R_{MS} (4.29) is demonstrated in Fig. 14.

Inclusion of island

Let us describe the island configuration for the finite region R_{MS} . In contrast to the region R_{AS} considered in Subsection 4.1, the interval $[\mathbf{b}_+^{\text{up}}, \mathbf{q}_+^{\text{up}}] \in R_{\text{MS}}$ in the right wedge is mirror-symmetric to the interval $[\mathbf{q}_-^{\text{up}}, \mathbf{b}_-^{\text{up}}] \in R_{\text{MS}}$ in the left one (see Fig. 13). Moreover, one can show that the entropy $S(R_{\text{MS}} \cup I)$ is symmetric under the permutation $a \leftrightarrow p, t_a \leftrightarrow t_p$ of the coordinates of the island boundaries (4.11). Therefore, we take a mirror-symmetric ansatz for I_{MS} , as in [18], i.e.

$$I_{\text{MS}} : \quad p = a, \quad t_p = t_a. \quad (4.35)$$

¹¹Of course, the eternal black hole radiates permanently, so the “first” particle of radiation means that one emitted after a certain moment, which we choose as $t = 0$.

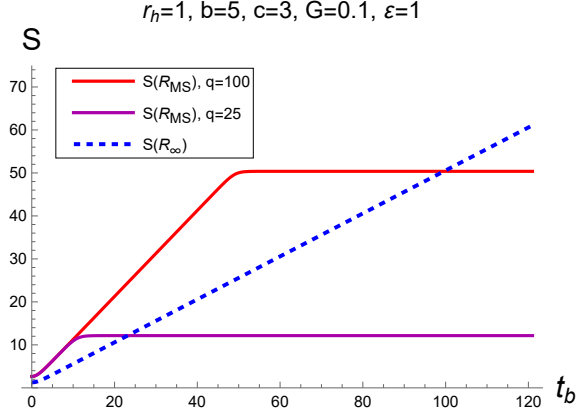


Figure 14: No-island entropy evolution for the finite region R_{MS} with $q = 25$ (darker magenta), $q = 100$ (red), and for the semi-infinite one R_∞ (blue dashed). For all cases, we take $b = 5$. The monotonic growth for the no-island entropy $S(R_{\text{MS}})$ is twice as fast compared to $S(R_\infty)$.

The generalized entropy before extremization is

$$S_I(R_{\text{MS}}) = \frac{\text{Area}(\partial I_{\text{MS}})}{4G} + S_{\text{matter}}(R_{\text{MS}} \cup I_{\text{MS}}). \quad (4.36)$$

The area term remains the same as in (4.19). The entanglement entropy $S_{\text{matter}}(R_{\text{MS}} \cup I_{\text{MS}})$ reads

$$S_{\text{matter}}(R_{\text{MS}} \cup I_{\text{MS}}) = \mathcal{X}(a, b, q, t_a, t_b). \quad (4.37)$$

The explicit form of \mathcal{X} (A.10) is given in Appendix A.

The entropy (4.36) is extremized with respect to a and t_a . In the limit $\mathbf{q}_\pm \rightarrow i^0$, the entropy before extremization (4.36) does not reduce to that for the semi-infinite regions [18]. Indeed, again due to (3.20)

$$\lim_{q \rightarrow \infty} S_I(R_{\text{MS}}) = S_I(R_\infty) + \frac{c}{3} \log \cosh \kappa_h t_b. \quad (4.38)$$

Let us consider relatively early times in the sense that

$$\cosh \kappa_h (r_*(q) - r_*(a)) \gg \cosh \kappa_h (t_a \pm t_b), \quad (4.39)$$

$$\cosh \kappa_h (r_*(q) - r_*(b)) \gg \cosh 2\kappa_h t_b. \quad (4.40)$$

Under these conditions, the entropy $S_I(R_{\text{MS}})$ takes the form

$$S_I(R_{\text{MS}}) \simeq \frac{2\pi a^2}{G} + \frac{c}{6} \log \left[\frac{64f(a)f(b)}{\kappa_h^6} \cosh^2 \kappa_h t_a \cosh^4 \kappa_h t_b \right] \\ + \frac{c}{3} \log \left[\frac{\cosh \kappa_h (r_*(a) - r_*(b)) - \cosh \kappa_h (t_a - t_b)}{\cosh \kappa_h (r_*(a) - r_*(b)) + \cosh \kappa_h (t_a + t_b)} \right]. \quad (4.41)$$

The extremization procedure for (4.41) is the same as in [18]. So, if along with (4.39) and (4.40) the condition (4.25) is satisfied, i.e.

$$\cosh \kappa_h (r_*(b) - r_*(a)) \ll \cosh \kappa_h (t_a + t_b) \ll \cosh \kappa_h (r_*(q) - r_*(a)), \quad (4.42)$$

then there is the following island solution

$$t_a = t_b, \quad (4.43) \\ a - r_h \ll r_h.$$

An approximate analytical expression for the entropy with an island (4.43) is given by

$$S_I(R_{\text{MS}}) \simeq \frac{2\pi r_h^2}{G} + \frac{c}{6} \left[\log \left(\frac{16r_h^3(b - r_h)^2}{b\varepsilon^4} \right) + \frac{b - r_h}{r_h} \right] \\ + \frac{c}{6} \log \left(\frac{4f(q) \cosh^2 \kappa_h t_b}{\kappa_h^2 \varepsilon^2} \right) - \frac{c}{3} e^{2\kappa_h t_b - \kappa_h (r_*(q) - r_*(b))}. \quad (4.44)$$

See Appendix A for the details of the derivation of (4.44). Note that the exponential growth associated with finite size effects is suppressed due to the condition (4.40), so the entropy with the island $S_I(R_{\text{MS}})$ grows only linearly.

The monotonic growth of the entropy (4.44) *with* the island is the same as for the entropy *without* it (2.19) for the semi-infinite regions R_∞ , and twice as slow compared to the entropy *without* the island (4.32) for the region R_{MS} . The qualitative picture can be explained as follows. Both entangled particles in a pair are trapped by the entangling region and the black hole interior when the outgoing Hawking mode is in the region R_{MS} . When the outgoing particle leaves this region, only the interior one is trapped by the island. So, there is the same growth as for the semi-infinite regions without islands (2.19) with the only difference that the interior modes are trapped instead of the outgoing ones for R_∞ .

Now consider the late time approximation, when the inequalities (4.39) and (4.40)

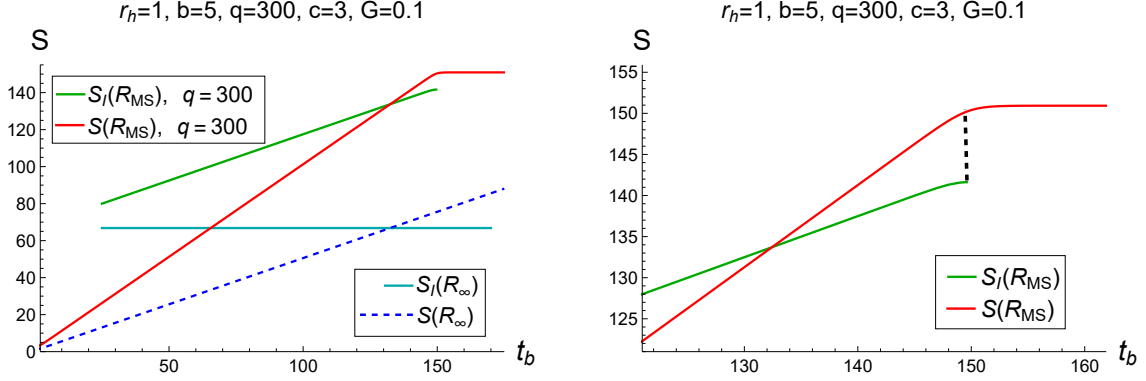


Figure 15: Entanglement entropy evolution for the finite size entangling region R_{MS} with $q = 300$, and for the infinite region R_∞ . For both cases we take $b = 5$. **Left:** the no-island entropy $S(R_{MS})$ (red), the entropy with the island $S_I(R_{MS})$ (green) for the same region R_{MS} ; the no-island entropy $S(R_\infty)$ (blue dotted) and the entanglement entropy $S_I(R_\infty)$ with the island (darker cyan) for the infinite region R_∞ . One can see that there is discrepancy between the entropies for the finite and infinite regions. **Right:** one can see that after the disappearance of the island for the region R_{MS} (green), there is an instantaneous transition to the no-island entropy (red).

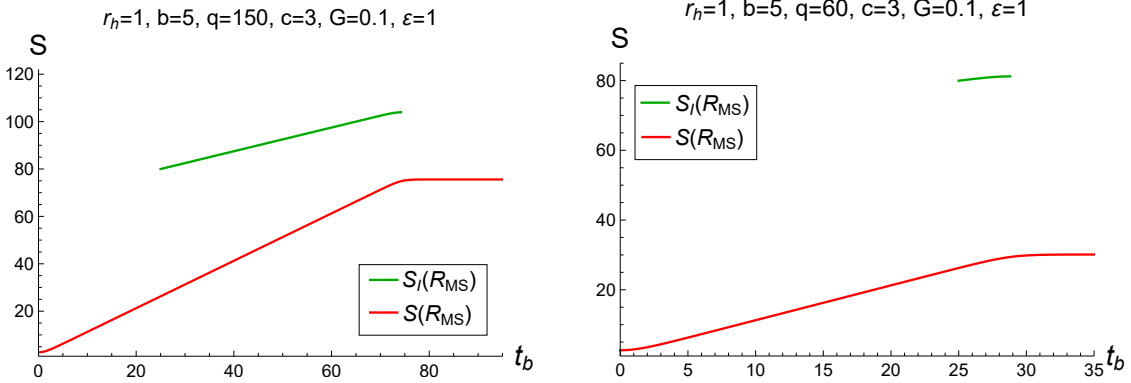


Figure 16: **Left:** entanglement entropy evolution for the region R_{MS} with $q = 150$ (red), and for the same region with the island I (green). **Right:** the same, but with $q = 60$. For both cases, we take $b = 5$. Notice that the entropy with the island I is not preferred by (2.15) over that for the no-island configuration R_{MS} .

hold in the opposite direction, i.e.

$$\begin{aligned} \cosh \kappa_h(t_a + t_b) &\gg \cosh \kappa_h(r_*(q) - r_*(a)), \\ \cosh 2\kappa_h t_b &\gg \cosh \kappa_h(r_*(q) - r_*(b)). \end{aligned} \quad (4.45)$$

Under these conditions, the entropy $S_I(R_{\text{MS}})$ is given by

$$S_I(R_{\text{MS}}) \simeq \frac{2\pi a^2}{G} + \frac{c}{3} \kappa_h t_a + \frac{c}{6} \log \left(\frac{4f(a)f(b)f(q)}{\kappa_h^6} \right) + \frac{c}{3} \log \left[\frac{(\cosh \kappa_h(r_*(a) - r_*(b)) - \cosh \kappa_h(t_a - t_b))(\cosh \kappa_h(r_*(b) - r_*(q)) - 1)}{\cosh \kappa_h(r_*(q) - r_*(a)) - \cosh \kappa_h(t_a - t_b)} \right]. \quad (4.46)$$

The entropy (4.46) grows monotonically with time t_a . It is obvious that there is no extremum over t_a , so the island exists only for finite time and, moreover, only if the two inequalities (4.42) hold simultaneously. One can see from (4.42) that by reducing the size of the finite region — by decreasing q or increasing b — it is possible to ensure that the inequalities cease to hold.

So, what features can be observed for the island dynamics when we consider R_{MS} ? Let us enumerate them and compare with the results obtained for R_{AS} :

- First of all, the breaking time does not make sense for R_{MS} — the interval is always spacelike. No-island entropy at large times is saturated at the value independent of time. The island, if it arises at all, exists for a finite time and disappears due to the violation of the extremization conditions (4.42). Numerical analysis shows (see Fig. 15 and Fig. 16) that the no-island entropy reaches the saturation at the time approximately equal to the moment of the disappearance of the island.
- The comparison of the entropies for R_{MS} and R_∞ shows that R_{MS} leads to a wrong entropy evolution in the large q limit, see Fig. 15 (left). Fig. 14 demonstrates that the monotonic growth for the no-island entropy $S(R_{\text{MS}})$ is twice as fast as for $S(R_\infty)$. The entropy with an island for the region R_{MS} grows monotonically with time, unlike R_∞ and R_{AS} .
- For large q , one can observe significant changes in the qualitative behaviour of the entropy for R_{MS} compared to R_{AS} . In Fig. 15 (right), after the disappearance of the island there is a discontinuous transition from the entropy with an island to the no-island entropy. In the next section, we will show that this behaviour causes the entanglement entropy to exceed the allowed upper bound. However, same as for R_{AS} , starting from relatively small values of q , the island never dominates, and the whole evolution corresponds to the no-island configuration (see Fig. 16).
- The island geometry for R_{MS} coincides with the one for R_∞ except for the moment when the island disappears (see Fig. 17).

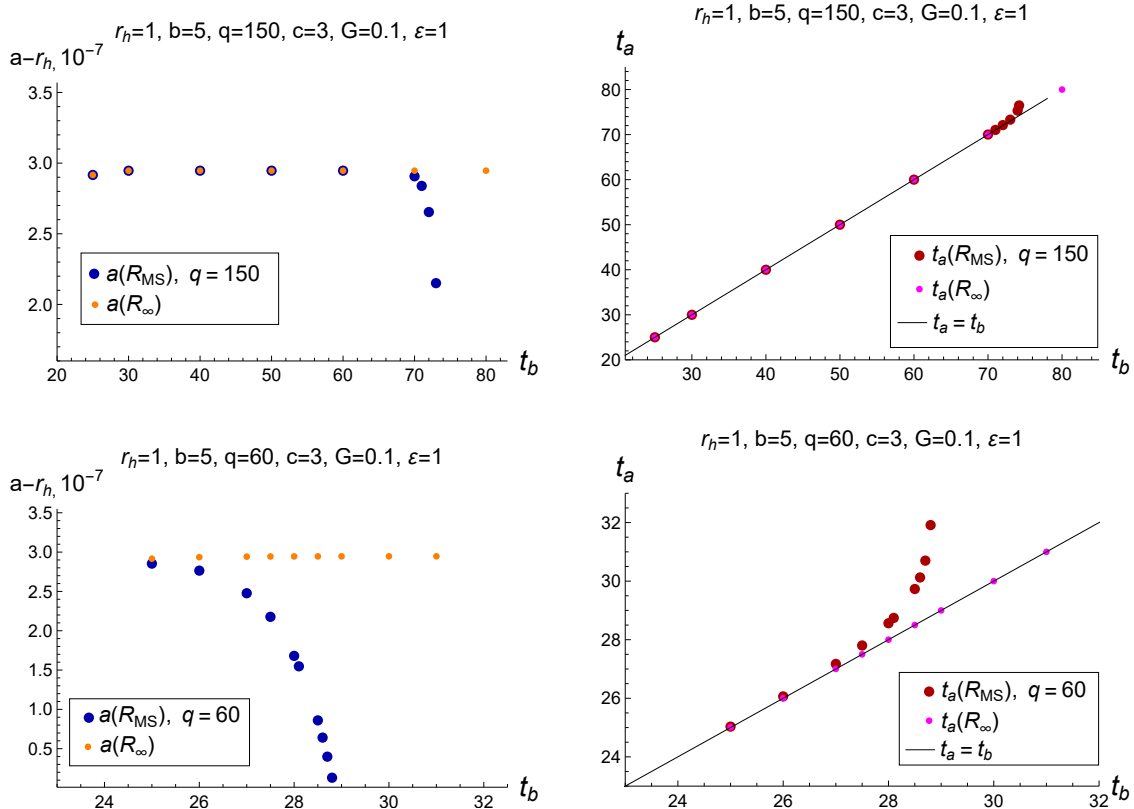


Figure 17: **Left:** evolution of the radial island coordinate a corresponding to the finite size entangling region R_{MS} (blue), and to the semi-infinite region R_∞ (orange). **Right:** evolution of the time island coordinate t_a corresponding to R_{MS} (magenta), and to R_∞ (pink). Just before the island disappearance, one can observe that the coordinates for the finite region R_{MS} cease to coincide with the coordinates of the infinite one R_∞ .

- Finally, as for R_{AS} , the lifetime of the island decreases with decreasing size of the region R_{MS} . Fig. 15 and Fig. 16 show this effect at a fixed b and decreasing q . Fig. 18 demonstrates the same for a fixed q and increasing b . For sufficiently large b and small q , the island does not appear at all.

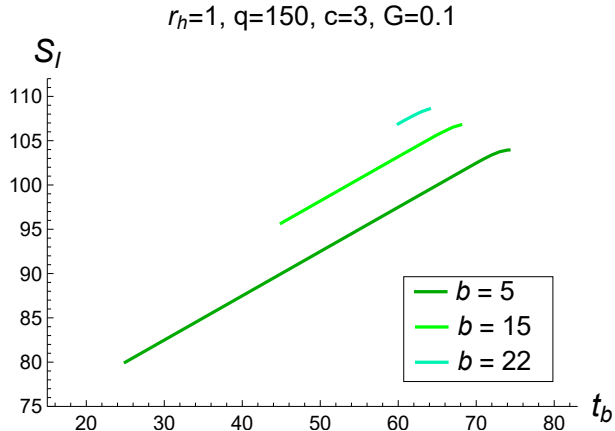


Figure 18: Time evolution of the entanglement entropy for $R_{\text{MS}} \cup I_{\text{MS}}$ with $b = 5$ (green), $b = 15$ (light green) and $b = 22$ (cyan).

5 Information loss paradox for finite entangling regions

In this section, we discuss how the Page curve [3, 4] of the two-sided Schwarzschild black hole gets modified for finite entangling regions. The expected early time dependence of the entanglement entropy for the eternal black hole is such that it grows until it reaches twice the value of the Bekenstein-Hawking entropy at the moment which is called the Page time. Taking an arbitrary moment of time as the starting point, the early time growth is due to increase of Hawking quanta number, entangled with the black hole, entering the entangling region. Subsequent behaviour of the Page curve for eternal black holes is to some extent a subject of uncertainties. We can definitely say only that if the fine-grained entropy exceeds the Bekenstein-Hawking entropy, then the paradox appears. The currently known island solution [18] fixes this problem by saturating the entropy at some fixed value which slightly exceeds the thermodynamical entropy (2.22).

We derive upper bounds following from the requirement that the entropy of the Schwarzschild black hole associated with the number of its microstates (fine-grained entropy) is to be constrained by the thermodynamical one (coarse-grained entropy) which is purely defined by its geometry. In the absence of entanglement islands, this upper bound for semi-infinite entangling regions is always violated during entanglement entropy evolution. We also give rise to a question whether entanglement islands actually heal the paradox if entangling regions are taken finite.

As a warm-up, let us remind the calculation of the upper bound on the entanglement entropy in the case of semi-infinite entangling regions where the Hawking radiation

of the eternal Schwarzschild black hole is collected¹². If the black hole and its radiation are in a pure quantum state, then the complementarity property (1.1) says that the fine-grained entropies (or the von Neumann entropies) for the black hole and radiation are equal

$$S(BH) = S(R_\infty), \quad (5.1)$$

where BH is the black hole entangling region.

The fine-grained entropy for the black hole should be bounded from above by the coarse-grained (thermodynamic) one

$$S(BH) \leq S^{\text{thermo}}(BH). \quad (5.2)$$

For the two-sided Schwarzschild black hole, its coarse-grained entropy is twice the Bekenstein-Hawking entropy $S_{\text{B-H}}$ [12, 18]

$$S^{\text{thermo}}(BH) = 2S_{\text{B-H}} = \frac{2\pi r_h^2}{G_N}. \quad (5.3)$$

Comparing (5.1), (5.2) and (5.3), we obtain the upper bound on the entanglement entropy of Hawking radiation

$$S(R_\infty) \leq \frac{2\pi r_h^2}{G_N}. \quad (5.4)$$

Violation of (5.4) means the Hawking information paradox¹³.

For the setup with the semi-infinite entangling region R_∞ , we neglect degrees of freedom of the radiation between the black hole horizon and the boundary surfaces \mathbf{b}_- and \mathbf{b}_+ (see Fig. 1 (left)). Then, the total Hilbert space \mathcal{H}_{tot} defined on some Cauchy surface $\Sigma \ni R_\infty$ can be partitioned into two parts: the first \mathcal{H}_{BH} is associated with the black hole, and the second \mathcal{H}_{R_∞} — with the collected radiation

$$\mathcal{H}_{\text{tot}} = \mathcal{H}_{BH} \otimes \mathcal{H}_{R_\infty}. \quad (5.5)$$

Let us now consider the finite region R (4.1) which collects the radiation between the boundaries \mathbf{b}_\pm and \mathbf{q}_\pm (see Fig. 1 (right)). In this case, the total Hilbert space \mathcal{H}_{tot} factorizes into three parts

$$\mathcal{H}_{\text{tot}} = \mathcal{H}_{BH} \otimes \mathcal{H}_R \otimes \mathcal{H}_C, \quad (5.6)$$

¹²For a comprehensive review of this topic see [25].

¹³More precisely, for the eternal Schwarzschild black hole, the information paradox is caused by an unstoppable increase of the entanglement entropy, the consequence of which is the exceeding of the Bekenstein-Hawking limit (5.4).

where $C = C_- \cup C_+$ is the entangling region which collects the radiation between \mathbf{q}_\pm and spacelike infinities i^0 of the corresponding wedges. This Hilbert space can also be rewritten as the following bipartitions¹⁴

$$\mathcal{H}_{\text{tot}} = \mathcal{H}_R \otimes \mathcal{H}_{BH \cup C} = \mathcal{H}_{BH} \otimes \mathcal{H}_{R \cup C} = \mathcal{H}_C \otimes \mathcal{H}_{BH \cup R}. \quad (5.7)$$

If we are given a pure quantum state in the total Hilbert space \mathcal{H}_{tot} , then from the complementarity property we have the following relations between the entropies of these bipartitions (5.7)

$$\begin{aligned} S(BH) &= S(R \cup C), \\ S(R) &= S(BH \cup C), \\ S(C) &= S(BH \cup R). \end{aligned} \quad (5.8)$$

Strong subadditivity of the entanglement entropy [75] for tripartitions like (5.6) gives the inequality

$$S(R \cup C \cup BH) + S(R) \leq S(BH \cup R) + S(R \cup C), \quad (5.9)$$

Taking into account (5.8) and the purity of the total state which means $S(R \cup C \cup BH) = 0$, we arrive at the following condition on the entropy for the finite region R

$$S(R) \leq S(BH) + S(C). \quad (5.10)$$

Therefore, combining (5.2), (5.3) and (5.10), we get an upper bound on the entanglement entropy for the finite region R

$$S(R) \leq \frac{2\pi r_h^2}{G_N} + S(C). \quad (5.11)$$

Exceeding the constraint (5.11) would signal about the information loss paradox for *finite* regions.

Note that for the semi-infinite region R_∞ [18], the generalized entropy (2.22) contains the terms caused by the inclusion of the entanglement island

$$S_{\text{gen}} \simeq S_{\text{B-H}} + \frac{c}{6} \left[\log \left(\frac{16r_h^3(b-r_h)^2}{\varepsilon^4 b} \right) + \frac{b-r_h}{r_h} \right] \equiv S_{\text{B-H}} + S_{\text{corr}}. \quad (5.12)$$

These corrections S_{corr} are small compared to the area term $S_{\text{B-H}}$ under the “black

¹⁴Here $\mathcal{H}_{X \cup Y} \equiv \mathcal{H}_X \otimes \mathcal{H}_Y$.

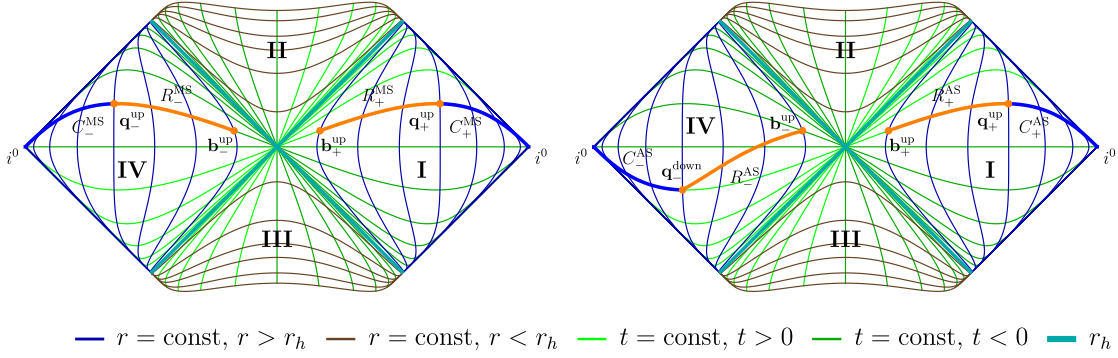


Figure 19: Left: Penrose diagram for the eternal Schwarzschild black hole with mirror-symmetric entangling region R_∞ partitioned into two subregions: $R_{\text{MS}} \equiv R_-^{\text{MS}} \cup R_+^{\text{MS}}$ and $C_{\text{MS}} \equiv C_-^{\text{MS}} \cup C_+^{\text{MS}}$. **Right:** the same diagram with asymmetric entangling region R_∞ partitioned into two subregions: $R_{\text{AS}} \equiv R_-^{\text{AS}} \cup R_+^{\text{AS}}$ and $C_{\text{AS}} \equiv C_-^{\text{AS}} \cup C_+^{\text{AS}}$. $C_+^{\text{MS/AS}}$ denote the region $[\mathbf{q}_+^{\text{up}}, i_0)$, and $C_-^{\text{MS/AS}} = [\mathbf{q}_-^{\text{up/down}}, i_0)$.

hole classicality” condition $r_h^2/G_N \gg c$. Therefore, the inequality (5.4) actually gets modified in the presence of the islands. If the entropy of the radiation exceeds the Bekenstein-Hawking limit $S_{\text{B-H}}$ only within the corridor $S_{\text{B-H}} \leq S \leq S_{\text{B-H}} + S_{\text{corr}}$ (5.12) as the evolution goes, we say that the inequality (5.4) still holds, and the information paradox does not arise.

In Section 4, we have considered two different types of finite entangling regions: R_{AS} (4.7) and R_{MS} (4.9). We denote the region C corresponding to R_{AS} as C_{AS} (see Fig. 19 (right)), and the one corresponding to R_{MS} as C_{MS} (see Fig. 19 (left)).

5.1 Asymmetric entangling region

Let us start with the region C_{AS} . Using AS regularization (see Subsection 3.5), one can show that

$$S(C_{\text{AS}}) = \frac{c}{6} \log \frac{4f(q)}{\kappa_h^2 \varepsilon^2}. \quad (5.13)$$

The entropy (5.13) does not depend on time. As we have seen in Section 4.1, there are two essentially different types of AS finite size configurations where the entanglement island either dominates in a finite time or does not dominate at all. To formulate our results more clear, let us call the first type the “large size” configurations, and the second one — the “small size” configurations. These names do not necessarily mean that $\mathbf{b}_\pm \ll \mathbf{q}_\pm$ or $\mathbf{b}_\pm \lesssim \mathbf{q}_\pm$ but rather classify different evolution patterns. Now we consider these cases separately.

Large size configurations

If we consider the configuration with an island for the semi-infinite region C_{AS} , then the entropy will be greater than (5.13) by the island area term of order r_h^2/G_N , which is much bigger in our approximation. Therefore, according to the island formula (2.15), the no-island entropy (5.13) dominates at all times. From (5.11), we get an upper bound on the entanglement entropy of Hawking radiation for the finite region R_{AS}

$$S(R_{AS}) \leq \frac{2\pi r_h^2}{G_N} + \frac{c}{6} \log \frac{4f(q)}{\kappa_h^2 \varepsilon^2}. \quad (5.14)$$

In Subsection 4.1, it was shown that the entropy with an island has the largest possible value (4.28) just before the rapid decrease around the breaking time

$$\begin{aligned} S_I(R_{AS}) \simeq & \frac{2\pi r_h^2}{G_N} + \frac{c}{6} \log \frac{4f(q)}{\kappa_h^2 \varepsilon^2} + \\ & + \frac{c}{6} \left[\log \left(\frac{16r_h^3(b-r_h)^2}{b\varepsilon^4} \right) + \frac{b-r_h}{r_h} \right] - \frac{c}{3} e^{2\kappa_h t_b - \kappa_h(r_*(q) - r_*(b))}. \end{aligned}$$

Therefore, we can use this value as the LHS of the inequality (5.14) to check its validity. The entropy $S_I(R_{AS})$ exceeds the RHS of (5.14) by the terms proportional to $c \ll r_h^2/G_N$. Therefore, we can say that the inequality (5.14) is satisfied approximately in the sense indicated above.

Small size configurations

The island contribution is of order of the Bekenstein-Hawking entropy S_{B-H} , and the entropy for AS no-island small size configurations dominates at all times, i.e. it is always smaller than that for the configurations with islands (see Fig. 10). It means that not only the inequality (5.14) is certainly satisfied, but also that the islands are not required for the resolution of the paradox.

5.2 Mirror-symmetric entangling region

Now let us consider the entropy for C_{MS} which was studied in [18]. Remind that at early times, the island is not formed and the entropy grows with time, while at late times, it saturates due to formation of the island

$$S(C_{MS}) = \begin{cases} \frac{c}{6} \log \left(\frac{4f(q) \cosh^2 \kappa_h t_q}{\kappa_h^2 \varepsilon^2} \right), & \text{early times,} \\ \frac{2\pi r_h^2}{G} + \frac{c}{6} \left[\log \left(\frac{16r_h^3(q-r_h)^2}{\varepsilon^4 q} \right) + \frac{q-r_h}{r_h} \right], & \text{late times.} \end{cases} \quad (5.15)$$

From (5.11), we get an upper bound on the entanglement entropy of Hawking radiation for a finite region R_{MS} for fixed q and relatively early times t_q as

$$S(R_{\text{MS}}) \leq \frac{2\pi r_h^2}{G} + \frac{c}{6} \log \left(\frac{4f(q) \cosh^2 \kappa_h t_q}{\kappa_h^2 \varepsilon^2} \right), \quad (5.16)$$

and for sufficiently large t_q as

$$S(R_{\text{MS}}) \leq \frac{4\pi r_h^2}{G} + \frac{c}{6} \left[\log \left(\frac{16r_h^3(q - r_h)^2}{\varepsilon^4 q} \right) + \frac{q - r_h}{r_h} \right]. \quad (5.17)$$

Under the condition $t_b = t_q$, time dependence of both entropies for R_{MS} and C_{MS} is determined by the same time coordinate t_b . However, the island dynamics is essentially different for semi-infinite and finite regions. As we have shown in Subsection 4.2, the entanglement island for a finite R_{MS} region exist only at the “intermediate” stage of the entropy evolution, namely, when approximately $b \ll t_b \ll q$. Let us cite the exact condition (4.42)

$$\cosh \kappa_h(r_*(b) - r_*(a^R)) \ll \cosh \kappa_h(t_a^R + t_b) \ll \cosh \kappa_h(r_*(q) - r_*(a^R)),$$

where a^R, t_a^R are the coordinates of the island boundaries associated with the region R_{MS} .

Since the boundaries \mathbf{q}_\pm are adjacent for R_{MS} and C_{MS} , they play opposite roles in the island formation for the semi-infinite region C_{MS} compared to R_{MS} . Namely, while for R_{MS} , q determines the time when the island I_R disappears (if it appears at all), for C_{MS} it defines the moment when the island I_C only emerges. As was shown in [18], for a semi-infinite region, the island solution can be found only at late times, which approximately mean $t_b \gg q$. The exact condition is

$$\cosh \kappa_h(t_b + t_a^C) \gg \cosh \kappa_h(r_*(q) - r_*(a^C)), \quad (5.18)$$

where a^C, t_a^C are the island coordinates for the region C_{MS} . By comparing these conditions (4.42) and (5.18), we clearly see that they cannot be obeyed together, therefore, islands for R_{MS} and C_{MS} do not exist simultaneously. It is important that first I_R appears (if R_{MS} is large enough for I_R to emerge), and only some time after I_R disappears, the island I_C is formed.

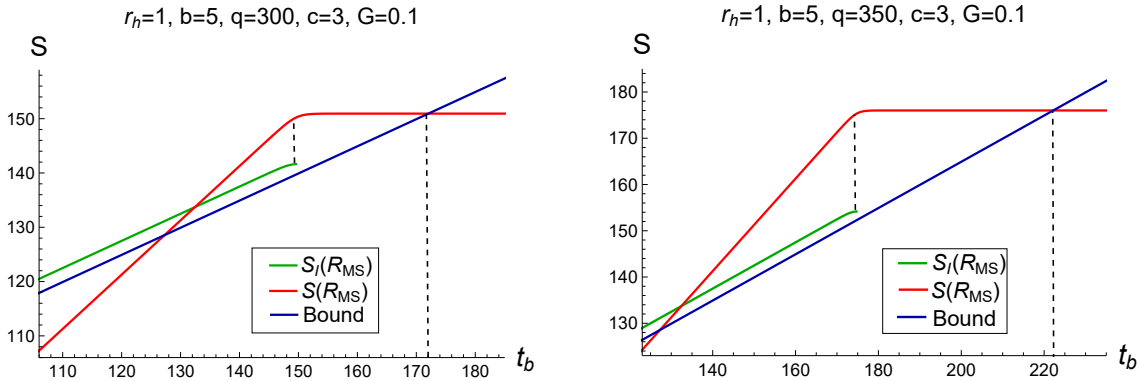


Figure 20: **Left:** Time evolution of the no-island entropy $S(R_{\text{MS}})$ (red), the entropy with the island $S_I(R_{\text{MS}})$ (green) and the upper bound (5.16) (blue) for the finite size entangling regions R_{MS} with $q = 300$. **Right:** the same, but with $q = 350$. For both cases, we take $b = 5$. After the disappearance of the island, there is a discontinuous transition to the no-island entropy $S(R_{\text{MS}})$, that during finite time (between two vertical shaded lines) is larger than the upper bound. One can see that as q increases, the difference between $S(R_{\text{MS}})$ and the upper bound increases, while the difference between $S_I(R_{\text{MS}})$ and the upper bound does not change significantly.

Large size configurations

For $q \gg b$, after the disappearance of I_R , one can show¹⁵ that I_C does not appear for a relatively long time. Therefore, the upper bound is given by the RHS of the inequality (5.16), and the entropy $S(R_{\text{MS}})$ on the LHS of (5.16) is that for the no-island configuration. However, the no-island entropy $S(R_{\text{MS}})$ grows twice as fast (4.32) as the RHS of (5.16). This means that at some point, the constraint (5.16) can no longer be satisfied (see Fig. 20). After the disappearance of I_R , there is a discontinuous transition to the constant value (4.34) of the no-island configuration. Therefore, for some time, the entropy $S(R_{\text{MS}})$ is significantly larger than the upper bound, and the bigger the value of q is — the longer the constraint is violated.

In Fig. 20, $S_I(R_{\text{MS}})$ is slightly larger than the upper bound, and this difference does not change significantly if we vary q ¹⁶. After the island disappearance, the difference between the no-island entropy $S(R_{\text{MS}})$ and the upper bound grows as q increases due to the increasing saturation value (4.34). Thus, we say that the inequality (5.16) is satisfied approximately for the entropy with an island $S_I(R_{\text{MS}})$ and is violated for a

¹⁵The entropy $S_I(C_{\text{MS}})$ with an island (5.15) takes relatively large values for large q due to the term proportional to q/r_h , so it starts to dominate at very late times.

¹⁶Indeed, the difference between $S_I(R_{\text{MS}})$ (4.44) and the RHS of (5.16) is approximately the same as the difference between the entropy with an island (2.22) for a semi-infinite region and the area term $2\pi r_h^2/G_N$, and does not change significantly as q increases.

finite time after I_R disappears.

As we have seen in Section 3.5, different regularization schemes lead to different behaviours of the entropy at spacelike infinity i^0 . In particular, the entropy for a semi-infinite region, calculated in the MS scheme which was implicitly assumed in [18], differs from that of the complementary region by a time-dependent function which grows with time. This fact raises the question about what result we would get for MS configurations in the context of the information paradox.

Consider the entropy for the region C_{MS} in the limit $\mathbf{q}_{\pm} \rightarrow i^0$. Effectively, it corresponds to vanishing C_{MS} and R_{MS} being semi-infinite. As a consequence, in this limit, there is no late time regime, as it can be seen from (5.18). Therefore, we assume that I_C appears only in the asymptotic future $t_b \rightarrow \infty$, and the no-island entropy $S(C_{\text{MS}})$ dominates at all finite times. Then, the upper bound on $S(R_{\text{MS}})$ is given by the inequality (5.16). Using MS regularization, we obtain from (5.16) at $\mathbf{q}_{\pm} \rightarrow i^0$

$$\lim_{\mathbf{q}_{\pm} \rightarrow i^0} S(R_{\text{MS}}) \leq \frac{2\pi r_h^2}{G} + \frac{c}{3} \log \cosh \kappa_h t_b. \quad (5.19)$$

The entropies $S(R_{\text{MS}})$ and $S_I(R_{\text{MS}})$ were found in Section 4.2, see (4.30) and (4.38)

$$\begin{aligned} \lim_{\mathbf{q}_{\pm} \rightarrow i^0} S(R_{\text{MS}}) &= S(R_{\infty}) + \frac{c}{3} \log \cosh \kappa_h t_b, \\ \lim_{\mathbf{q}_{\pm} \rightarrow i^0} S_I(R_{\text{MS}}) &= S_I(R_{\infty}) + \frac{c}{3} \log \cosh \kappa_h t_b. \end{aligned}$$

If we substitute either $S(R_{\text{MS}})$ or $S_I(R_{\text{MS}})$ in the limit $\mathbf{q}_{\pm} \rightarrow i^0$ in (5.19), we will see that the time-dependent terms cancel, and the upper bound on semi-infinite MS regions (5.4) is also satisfied. Note that this statement does not contradict our previous result that for large but finite q , the entropy exceeds the upper bound — this is because there is no discontinuous transition in $S(R_{\text{MS}})$ in the limit $\mathbf{q}_{\pm} \rightarrow i^0$ at any finite time.

Small size configurations

As in the case with R_{AS} , for relatively small sizes of the region R_{MS} , the no-island entropy always dominates and does not exceed the entropy with an island. Therefore, for small regions, the inequalities (5.16) and (5.17) are satisfied unconditionally.

Summary

Let us summarize our findings:

- For the eternal Schwarzschild black hole, we obtained the upper bound (5.11) on the entanglement entropy of Hawking radiation collected in an arbitrary finite region R . The upper bound is determined by the thermodynamic entropy for the two-sided black hole and the entanglement entropy for the semi-infinite region C which collects radiation outside R . We considered two types of finite regions — R_{AS} with a finite lifetime and R_{MS} located between two concentric spheres at constant time.
- For both types, if the size of R is small in the sense that the configuration with an island is not dominant during the entire evolution, the entropy does not exceed the upper bound (5.11). Thus, such small regions do not require the island prescription to avoid the information paradox. Also, for both types at $\mathbf{q}_{\pm} \rightarrow i^0$, the upper bound condition for semi-infinite regions is reproduced, and in this case, the introduction of islands is necessary.
- For sufficiently large regions R_{AS} , the presence of islands leads to the fact that the entropy does not exceed the upper bound (5.11).
- With regard to the large but finite regions R_{MS} at late times, their entropy exceeds the upper bound for a finite time (see Fig. 20) due to the discontinuous transition to the no-island configuration after the island disappears. Thus, the island prescription for R_{MS} does not in general solve the information paradox.

6 Conclusions & Future prospects

In this paper, we address the properties of the entanglement entropy of Hawking radiation on the background of the eternal Schwarzschild black hole in the case of entangling regions of finite size. Not only this knowledge itself is necessary for IR regularizations in the context of the information paradox, but it is also vital for spacetimes with finite observable domains. Among them are de Sitter (dS) and Schwarzschild-de Sitter (SdS) solutions where a physical observer is bounded within the cosmological horizon. Therefore, only finite entangling regions are of physical significance in these spacetimes, and we are going to generalise the results of this paper on dS and SdS cases in the forthcoming paper.

We have established different ways of choosing finite entangling regions in Schwarzschild spacetime and demonstrated that only the asymmetric regularization is consistent with the complementarity property of the entanglement entropy. However, the corresponding Cauchy surface is no longer “immortal” and has a finite lifetime depending on the size of the entangling region. In this case, one gets a typical Hawking paradox: a linear growth of the entropy with time and the excess of the Bekenstein-Hawking entropy — with the only qualitative difference that right before the breaking time the entropy falls extremely fast.

Also, we have derived the constraints on the entanglement entropy for different choices of entangling regions. It turns out that the upper bound on the entropy for a finite region depends on the size of this region and on the location of its endpoints.

Accounting for the entanglement islands proves to be consistent with the unitarity of entropy evolution in the case of the asymmetric regularization. It preserves the conservation of information, thus, no paradoxes arise. However, the entanglement entropy might violate the upper bound inequalities for other choices of the entangling regions even in the presence of the islands.

Acknowledgements

We would like to thank M. Khramtsov and I. Volovich for useful discussions. DA, IA, AE and TR are supported by the Russian Science Foundation (project 20-12-00200, Steklov Mathematical Institute).

Appendix

A Explicit formulas for entanglement entropy with island

In this appendix, we present the explicit formulas for the matter contribution to the generalized entropy (2.15).

Asymmetric region

The entanglement entropy of conformal matter for $R_{\text{AS}} \cup I$ is

$$S_{\text{matter}}(R_{\text{AS}} \cup I) = \mathcal{Y}(a, p, b, q, t_a, t_p, t_b), \quad (\text{A.1})$$

where $\mathcal{Y}(a, p, b, q, t_a, t_p, t_b)$ is given by

$$\begin{aligned} \mathcal{Y}(a, p, b, q, t_a, t_p, t_b) = & \frac{c}{6} \log \left[\frac{(\cosh \kappa_h(r_*(b) - r_*(q)) - \cosh 2\kappa_h t_b)(\cosh \kappa_h(r_*(b) - r_*(q)) - 1)}{(\cosh \kappa_h(r_*(b) - r_*(q)) + \cosh 2\kappa_h t_b)(\cosh \kappa_h(r_*(b) - r_*(q)) + 1)} \right] \\ & + \frac{c}{6} \log \left[\frac{(\cosh \kappa_h(r_*(a) - r_*(b)) - \cosh \kappa_h(t_a - t_b))(\cosh \kappa_h(r_*(p) - r_*(b)) - \cosh \kappa_h(t_p - t_b))}{(\cosh \kappa_h(r_*(a) - r_*(b)) + \cosh \kappa_h(t_a + t_b))(\cosh \kappa_h(r_*(p) - r_*(b)) + \cosh \kappa_h(t_p + t_b))} \right] \\ & + \frac{c}{6} \log \left[\frac{(\cosh \kappa_h(r_*(a) - r_*(q)) + \cosh \kappa_h(t_a - t_b))(\cosh \kappa_h(r_*(p) - r_*(q)) + \cosh \kappa_h(t_p + t_b))}{(\cosh \kappa_h(r_*(a) - r_*(q)) - \cosh \kappa_h(t_a - t_b))(\cosh \kappa_h(r_*(p) - r_*(q)) - \cosh \kappa_h(t_p + t_b))} \right] \\ & + \frac{c}{6} \log \left[\frac{32\sqrt{f(a)f(p)f(b)f(q)}}{\kappa_h^6 \varepsilon^6} \cosh^2 \kappa_h t_b (\cosh \kappa_h(r_*(a) - r_*(p)) + \cosh \kappa_h(t_a + t_p)) \right]. \end{aligned} \quad (\text{A.2})$$

Let us obtain an approximate analytical expression for the entropy (A.2) at times long before the breaking time, when a symmetric island (4.27) with its boundaries near the horizon emerges, i.e. when

$$\cosh \kappa_h(r_*(b) - r_*(a)) \ll \cosh 2\kappa_h t_b \ll \cosh \kappa_h(r_*(q) - r_*(b)). \quad (\text{A.3})$$

Note that the inequality

$$\cosh 2\kappa_h t_b \ll \cosh \kappa_h(r_*(q) - r_*(a)) \quad (\text{A.4})$$

follows from (A.3) due to the fact that $r_*(b) \gg r_*(a)$ in the near-horizon zone.

The entropy (A.2) under the symmetric island ansatz (4.27) is

$$\begin{aligned}
\mathcal{Y}(a, a, b, q, t_b, t_b, t_b) &= \frac{c}{6} \log \left[\frac{(\cosh \kappa_h(r_*(b) - r_*(q)) - \cosh 2\kappa_h t_b)(\cosh \kappa_h(r_*(b) - r_*(q)) - 1)}{(\cosh \kappa_h(r_*(b) - r_*(q)) + \cosh 2\kappa_h t_b)(\cosh \kappa_h(r_*(b) - r_*(q)) + 1)} \right] \\
&+ \frac{c}{6} \log \left[\frac{(\cosh \kappa_h(r_*(a) - r_*(q)) + \cosh 2\kappa_h t_b)(\cosh \kappa_h(r_*(a) - r_*(q)) + 1)}{(\cosh \kappa_h(r_*(a) - r_*(q)) - \cosh 2\kappa_h t_b)(\cosh \kappa_h(r_*(a) - r_*(q)) - 1)} \right] \\
&+ \frac{c}{6} \log \left[\frac{64f(a)f(b)f(q)}{\kappa_h^6 \varepsilon^6} \cosh^4 \kappa_h t_b \right] + \frac{c}{3} \log \left[\frac{\cosh \kappa_h(r_*(a) - r_*(b)) - 1}{\cosh \kappa_h(r_*(a) - r_*(b)) + \cosh 2\kappa_h t_b} \right].
\end{aligned} \tag{A.5}$$

It can be seen that under the conditions (A.3) and (A.4), the entropy (A.5) simplifies as¹⁷

$$\begin{aligned}
\mathcal{Y} &\simeq \frac{c}{6} \log \left[\frac{4f(a)f(b)f(q)}{\kappa_h^6 \varepsilon^6} \right] + \frac{c}{3} \kappa_h(r_*(b) - r_*(a)) - \frac{2c}{3} e^{-\kappa_h(r_*(b) - r_*(a))} - \frac{c}{3} e^{-2\kappa_h t_b + \kappa_h(r_*(b) - r_*(a))} \\
&- \frac{c}{3} \left[e^{2\kappa_h t_b - \kappa_h(r_*(q) - r_*(b))} + 2e^{-\kappa_h(r_*(q) - r_*(b))} - e^{2\kappa_h t_b - \kappa_h(r_*(q) - r_*(a))} - 2e^{-\kappa_h(r_*(q) - r_*(a))} \right].
\end{aligned} \tag{A.6}$$

All the exponential terms in the considered approximations are negligible. We take into account only the largest exponential term related to the finite size effect for the entangling region. It is possible to find an analytical expression for the entropy (A.6) without an explicit form of the radial coordinate of the island boundary $a = r_h + X$ in the leading order in X/r_h from the near-horizon zone assumption. With the use of (A.6), one can obtain

$$\mathcal{Y} \simeq \frac{c}{6} \left[\log \left(\frac{16r_h^3(b - r_h)^2}{b\varepsilon^4} \right) + \frac{b - r_h}{r_h} \right] + \frac{c}{6} \log \left(\frac{4f(q)}{\kappa_h^2 \varepsilon^2} \right) - \frac{c}{3} e^{2\kappa_h t_b - \kappa_h(r_*(q) - r_*(b))}. \tag{A.7}$$

The area term (4.19) in the leading order in X/r_h is

$$\frac{\text{Area}(\partial I)}{4G} \simeq \frac{2\pi r_h^2}{G}. \tag{A.8}$$

Mirror-symmetric region

The entanglement entropy of conformal matter for $R_{\text{MS}} \cup I_{\text{MS}}$ has the following form

$$S_{\text{matter}}(R_{\text{MS}} \cup I_{\text{MS}}) = \mathcal{X}(a, b, q, t_a, t_b), \tag{A.9}$$

¹⁷In (A.6), we use the fact that $\cosh x \simeq \frac{1}{2}e^x$ at $x \gg 1$.

where $\mathcal{X}(a, b, q, t_a, t_b)$ is

$$\begin{aligned}
\mathcal{X}(a, b, q, t_a, t_b) &= \frac{c}{6} \log \left[\frac{64f(a)f(b)f(q)}{\kappa_h^6 \varepsilon^6} \cosh^2 \kappa_h t_a \cosh^4 \kappa_h t_b \right] \\
&+ \frac{c}{3} \log \left[\frac{(\cosh \kappa_h(r_*(b) - r_*(a)) - \cosh \kappa_h(t_a - t_b)) (\cosh \kappa_h(r_*(q) - r_*(a)) + \cosh \kappa_h(t_a + t_b))}{(\cosh \kappa_h(r_*(b) - r_*(a)) + \cosh \kappa_h(t_a + t_b)) (\cosh \kappa_h(r_*(q) - r_*(a)) - \cosh \kappa_h(t_a - t_b))} \right] \\
&+ \frac{c}{3} \log \left[\frac{\cosh \kappa_h(r_*(b) - r_*(q)) - 1}{\cosh \kappa_h(r_*(b) - r_*(q)) + \cosh 2\kappa_h t_b} \right].
\end{aligned} \tag{A.10}$$

Let us obtain an approximate analytical expression for the entropy (A.10) under the conditions (4.42), when there is an island (4.43) in the near-horizon zone. Performing similar calculations as in the derivation of (A.7), one can obtain for $\mathcal{X}(a, b, q, t_b, t_b)$ in the leading order in X/r_h

$$\mathcal{X} \simeq \frac{c}{6} \left[\log \left(\frac{16r_h^3(b - r_h)^2}{b\varepsilon^4} \right) + \frac{b - r_h}{r_h} \right] + \frac{c}{6} \log \left(\frac{4f(q) \cosh^2 \kappa_h t_b}{\kappa_h^2 \varepsilon^2} \right) - \frac{c}{3} e^{2\kappa_h t_b - \kappa_h(r_*(q) - r_*(b))}. \tag{A.11}$$

The area term in the leading order in X/r_h for the region R_{MS} coincides with (A.8).

References

- [1] S.W. Hawking, “Particle creation by black holes,” *Comm. Math. Phys.* **43** (1975) 199.
- [2] S.W. Hawking, “Breakdown of Predictability in Gravitational Collapse,” *Phys. Rev. D* **14**, 2460-2473 (1976).
- [3] D. N. Page, “Information in black hole radiation,” *Phys. Rev. Lett.* **71**, 3743-3746 (1993) [arXiv:hep-th/9306083 [hep-th]].
- [4] D. N. Page, “Time Dependence of Hawking Radiation Entropy,” *JCAP* **1309**, 028 (2013) [arXiv:1301.4995 [hep-th]].
- [5] G. Penington, “Entanglement Wedge Reconstruction and the Information Paradox,” *JHEP* **09**, 002 (2020) [arXiv:1905.08255 [hep-th]].
- [6] A. Almheiri, N. Engelhardt, D. Marolf and H. Maxfield, “The entropy of bulk quantum fields and the entanglement wedge of an evaporating black hole,” *JHEP* **12**, 063 (2019) [arXiv:1905.08762 [hep-th]].
- [7] A. Almheiri, R. Mahajan, J. Maldacena and Y. Zhao, “The Page curve of Hawking radiation from semiclassical geometry,” *JHEP* **03**, 149 (2020) doi:10.1007/JHEP03(2020)149 [arXiv:1908.10996 [hep-th]].
- [8] P. C. W. Davies and S. A. Fulling, “Radiation from a moving mirror in two-dimensional space-time conformal anomaly,” *Proc. Roy. Soc. Lond. A* **348**, 393-414 (1976)
- [9] M. R. R. Good, K. Yelshibekov and Y. C. Ong, “On Horizonless Temperature with an Accelerating Mirror,” *JHEP* **03**, 013 (2017) [arXiv:1611.00809 [gr-qc]].
- [10] P. Chen and D. h. Yeom, “Entropy evolution of moving mirrors and the information loss problem,” *Phys. Rev. D* **96**, no.2, 025016 (2017) [arXiv:1704.08613 [hep-th]].
- [11] M. R. R. Good, E. V. Linder and F. Wilczek, “Moving mirror model for quasithermal radiation fields,” *Phys. Rev. D* **101**, no.2, 025012 (2020) [arXiv:1909.01129 [gr-qc]].
- [12] A. Almheiri, R. Mahajan and J. Maldacena, “Islands outside the horizon,” [arXiv:1910.11077 [hep-th]].
- [13] M. Rozali, J. Sully, M. Van Raamsdonk, C. Waddell and D. Wakeham, “Information radiation in BCFT models of black holes,” *JHEP* **05**, 004 (2020) [arXiv:1910.12836 [hep-th]].
- [14] G. Penington, S. H. Shenker, D. Stanford and Z. Yang, “Replica wormholes and the black hole interior,” *JHEP* **03**, 205 (2022) [arXiv:1911.11977 [hep-th]].
- [15] A. Almheiri, T. Hartman, J. Maldacena, E. Shaghoulian and A. Tajdini, “Replica Wormholes and the Entropy of Hawking Radiation,” *JHEP* **05**, 013 (2020) [arXiv:1911.12333 [hep-th]].

- [16] F. F. Gautason, L. Schneiderbauer, W. Sybesma and L. Thorlacius, “Page Curve for an Evaporating Black Hole,” *JHEP* **05**, 091 (2020) [arXiv:2004.00598 [hep-th]].
- [17] T. Anegawa and N. Iizuka, “Notes on islands in asymptotically flat 2d dilaton black holes,” *JHEP* **07**, 036 (2020) [arXiv:2004.01601 [hep-th]].
- [18] K. Hashimoto, N. Iizuka and Y. Matsuo, “Islands in Schwarzschild black holes,” *JHEP* **06**, 085 (2020) [arXiv:2004.05863 [hep-th]].
- [19] J. Sully, M. V. Raamsdonk and D. Wakeham, “BCFT entanglement entropy at large central charge and the black hole interior,” *JHEP* **03**, 167 (2021) [arXiv:2004.13088 [hep-th]].
- [20] T. Hartman, E. Shaghoulian and A. Strominger, “Islands in Asymptotically Flat 2D Gravity,” *JHEP* **07**, 022 (2020) [arXiv:2004.13857 [hep-th]].
- [21] C. Krishnan, V. Patil and J. Pereira, “Page Curve and the Information Paradox in Flat Space,” [arXiv:2005.02993 [hep-th]].
- [22] M. Alishahiha, A. Faraji Astaneh and A. Naseh, “Island in the presence of higher derivative terms,” *JHEP* **02**, 035 (2021) [arXiv:2005.08715 [hep-th]].
- [23] H. Geng and A. Karch, “Massive islands,” *JHEP* **09**, 121 (2020) [arXiv:2006.02438 [hep-th]].
- [24] H. Z. Chen, R. C. Myers, D. Neuenfeld, I. A. Reyes and J. Sandor, “Quantum Extremal Islands Made Easy, Part I: Entanglement on the Brane,” *JHEP* **10**, 166 (2020) [arXiv:2006.04851 [hep-th]].
- [25] A. Almheiri, T. Hartman, J. Maldacena, E. Shaghoulian and A. Tajdini, “The entropy of Hawking radiation,” *Rev. Mod. Phys.* **93** (2021) no.3, 035002 [arXiv:2006.06872 [hep-th]].
- [26] X. Dong, X. L. Qi, Z. Shangnan and Z. Yang, “Effective entropy of quantum fields coupled with gravity,” *JHEP* **10**, 052 (2020) [arXiv:2007.02987 [hep-th]].
- [27] V. Balasubramanian, A. Kar and T. Ugajin, “Islands in de Sitter space,” *JHEP* **02**, 072 (2021) [arXiv:2008.05275 [hep-th]].
- [28] H. Z. Chen, R. C. Myers, D. Neuenfeld, I. A. Reyes and J. Sandor, “Quantum Extremal Islands Made Easy, Part II: Black Holes on the Brane,” *JHEP* **12**, 025 (2020) [arXiv:2010.00018 [hep-th]].
- [29] Y. Ling, Y. Liu and Z. Y. Xian, “Island in Charged Black Holes,” *JHEP* **03**, 251 (2021) [arXiv:2010.00037 [hep-th]].
- [30] Y. Matsuo, “Islands and stretched horizon,” *JHEP* **07**, 051 (2021) [arXiv:2011.08814 [hep-th]].

- [31] K. Goto, T. Hartman and A. Tajdini, “Replica wormholes for an evaporating 2D black hole,” *JHEP* **04**, 289 (2021) doi:10.1007/JHEP04(2021)289 [arXiv:2011.09043 [hep-th]].
- [32] I. Akal, Y. Kusuki, N. Shiba, T. Takayanagi and Z. Wei, “Entanglement Entropy in a Holographic Moving Mirror and the Page Curve,” *Phys. Rev. Lett.* **126**, no.6, 061604 (2021) [arXiv:2011.12005 [hep-th]].
- [33] H. Geng, A. Karch, C. Perez-Pardavila, S. Raju, L. Randall, M. Riojas and S. Shashi, “Information Transfer with a Gravitating Bath,” *SciPost Phys.* **10**, no.5, 103 (2021) [arXiv:2012.04671 [hep-th]].
- [34] G. K. Karananas, A. Kehagias and J. Taskas, “Islands in linear dilaton black holes,” *JHEP* **03**, 253 (2021) [arXiv:2101.00024 [hep-th]].
- [35] X. Wang, R. Li and J. Wang, “Islands and Page curves of Reissner-Nordström black holes,” *JHEP* **04**, 103 (2021) [arXiv:2101.06867 [hep-th]].
- [36] K. Kawabata, T. Nishioka, Y. Okuyama and K. Watanabe, “Probing Hawking radiation through capacity of entanglement,” *JHEP* **05**, 062 (2021) [arXiv:2102.02425 [hep-th]].
- [37] I. A. Reyes, “Moving Mirrors, Page Curves, and Bulk Entropies in AdS₂,” *Phys. Rev. Lett.* **127**, no.5, 051602 (2021) [arXiv:2103.01230 [hep-th]].
- [38] H. Geng, Y. Nomura and H. Y. Sun, “Information paradox and its resolution in de Sitter holography,” *Phys. Rev. D* **103**, no.12, 126004 (2021) [arXiv:2103.07477 [hep-th]].
- [39] A. Bhattacharya, A. Bhattacharyya, P. Nandy and A. K. Patra, “Islands and complexity of eternal black hole and radiation subsystems for a doubly holographic model,” *JHEP* **05** (2021), 135 [arXiv:2103.15852 [hep-th]].
- [40] W. Kim and M. Nam, “Entanglement entropy of asymptotically flat non-extremal and extremal black holes with an island,” *Eur. Phys. J. C* **81**, no.10, 869 (2021) [arXiv:2103.16163 [hep-th]].
- [41] H. Geng, S. Lüster, R. K. Mishra and D. Wakeham, “Holographic BCFTs and Communicating Black Holes,” [arXiv:2104.07039 [hep-th]].
- [42] Y. Lu and J. Lin, “Islands in Kaluza–Klein black holes,” *Eur. Phys. J. C* **82**, no.2, 132 (2022) [arXiv:2106.07845 [hep-th]].
- [43] I. Akal, Y. Kusuki, N. Shiba, T. Takayanagi and Z. Wei, “Holographic moving mirrors,” *Class. Quant. Grav.* **38**, no.22, 224001 (2021) [arXiv:2106.11179 [hep-th]].
- [44] M. H. Yu and X. H. Ge, “Islands and Page curves in charged dilaton black holes,” *Eur. Phys. J. C* **82**, no.1, 14 (2022) [arXiv:2107.03031 [hep-th]].
- [45] H. Geng, A. Karch, C. Perez-Pardavila, S. Raju, L. Randall, M. Riojas and S. Shashi, “Inconsistency of islands in theories with long-range gravity,” *JHEP* **01**, 182 (2022) [arXiv:2107.03390 [hep-th]].

- [46] B. Ahn, S. E. Bak, H. S. Jeong, K. Y. Kim and Y. W. Sun, “Islands in charged linear dilaton black holes,” *Phys. Rev. D* **105**, no.4, 046012 (2022) [arXiv:2107.07444 [hep-th]].
- [47] D. S. Ageev, “Shaping contours of entanglement islands in BCFT,” *JHEP* **03**, 033 (2022) [arXiv:2107.09083 [hep-th]].
- [48] V. Balasubramanian, B. Craps, M. Khramtsov and E. Shaghoulian, “Submerging islands through thermalization,” *JHEP* **10**, 048 (2021) [arXiv:2107.14746 [hep-th]].
- [49] N. H. Cao, “Entanglement entropy and Page curve of black holes with island in massive gravity,” *Eur. Phys. J. C* **82**, no.4, 381 (2022) [arXiv:2108.10144 [hep-th]].
- [50] D. Fernández-Silvestre, J. Foo and M. R. R. Good, “On the duality of Schwarzschild–de Sitter spacetime and moving mirror,” *Class. Quant. Grav.* **39**, no.5, 055006 (2022) [arXiv:2109.04147 [gr-qc]].
- [51] S. Azarnia, R. Fareghbal, A. Naseh and H. Zolfi, “Islands in flat-space cosmology,” *Phys. Rev. D* **104**, no.12, 126017 (2021) [arXiv:2109.04795 [hep-th]].
- [52] A. Bhattacharya, A. Bhattacharyya, P. Nandy and A. K. Patra, “Partial islands and subregion complexity in geometric secret-sharing model,” *JHEP* **12** (2021), 091 [arXiv:2109.07842 [hep-th]].
- [53] I. Aref’eva and I. Volovich, “A Note on Islands in Schwarzschild Black Holes,” [arXiv:2110.04233 [hep-th]].
- [54] S. He, Y. Sun, L. Zhao and Y. X. Zhang, “The universality of islands outside the horizon,” *JHEP* **05**, 047 (2022) [arXiv:2110.07598 [hep-th]].
- [55] D. S. Ageev, I. Y. Aref’eva and A. V. Lysukhina, “Wormholes in Jackiw–Teitelboim Gravity,” *Teor. Mat. Fiz.* **201**, no.3, 424-439 (2019).
- [56] F. Omid, “Entropy of Hawking radiation for two-sided hyperscaling violating black branes,” *JHEP* **04** (2022), 022 [arXiv:2112.05890 [hep-th]].
- [57] A. Bhattacharya, A. Bhattacharyya, P. Nandy and A. K. Patra, “Bath deformations, islands, and holographic complexity,” *Phys. Rev. D* **105** (2022) no.6, 066019 [arXiv:2112.06967 [hep-th]].
- [58] H. Geng, A. Karch, C. Perez-Pardavila, S. Raju, L. Randall, M. Riojas and S. Shashi, “Entanglement phase structure of a holographic BCFT in a black hole background,” *JHEP* **05**, 153 (2022) [arXiv:2112.09132 [hep-th]].
- [59] M. H. Yu, C. Y. Lu, X. H. Ge and S. J. Sin, “Island, Page curve, and superradiance of rotating BTZ black holes,” *Phys. Rev. D* **105**, no.6, 6 (2022) [arXiv:2112.14361 [hep-th]].
- [60] K. Suzuki and T. Takayanagi, “BCFT and Islands in two dimensions,” *JHEP* **06**, 095 (2022) [arXiv:2202.08462 [hep-th]].

- [61] Q. L. Hu, D. Li, R. X. Miao and Y. Q. Zeng, “AdS/BCFT and Island for curvature-squared gravity,” *JHEP* **09**, 037 (2022) [arXiv:2202.03304 [hep-th]].
- [62] P. J. Hu, D. Li and R. X. Miao, [arXiv:2208.11982 [hep-th]].
- [63] I. Aref’eva, T. Rusalev and I. Volovich, “Entanglement entropy of near-extremal black hole,” [arXiv:2202.10259 [hep-th]].
- [64] W. C. Gan, D. H. Du and F. W. Shu, “Island and Page curve for one-sided asymptotically flat black hole,” *JHEP* **07**, 020 (2022) [arXiv:2203.06310 [hep-th]].
- [65] J. Basak Kumar, D. Basu, V. Malvimat, H. Parihar and G. Sengupta, “Reflected Entropy and Entanglement Negativity for Holographic Moving Mirrors,” [arXiv:2204.06015 [hep-th]].
- [66] S. Azarnia and R. Fareghbal, “Islands in Kerr–de Sitter spacetime and their flat limit,” *Phys. Rev. D* **106**, no.2, 026012 (2022) [arXiv:2204.08488 [hep-th]].
- [67] I. Akal, T. Kawamoto, S. M. Ruan, T. Takayanagi and Z. Wei, “Zoo of holographic moving mirrors,” [arXiv:2205.02663 [hep-th]].
- [68] M. Afrasiar, J. Kumar Basak, A. Chandra and G. Sengupta, “Islands for Entanglement Negativity in Communicating Black Holes,” [arXiv:2205.07903 [hep-th]].
- [69] A. Anand, “Page Curve and Island in EGB gravity,” [arXiv:2205.13785 [hep-th]].
- [70] D. S. Ageev and I. Y. Aref’eva, “Thermal density matrix breaks down the Page curve,” [arXiv:2206.04094 [hep-th]].
- [71] S. Djordjević, A. Gočanin, D. Gočanin and V. Radovanović, “Page Curve for Eternal Schwarzschild Black Hole in Dimensionally-Reduced Model of Dilaton Gravity,” [arXiv:2207.07409 [hep-th]].
- [72] K. Goswami and K. Narayan, “Small Schwarzschild de Sitter black holes, quantum extremal surfaces and islands,” [arXiv:2207.10724 [hep-th]].
- [73] A. Roy Chowdhury, A. Saha and S. Gangopadhyay, “The role of mutual information in the Page curve,” [arXiv:2207.13029 [hep-th]].
- [74] H. Geng, L. Randall and E. Swanson, “BCFT in a Black Hole Background: An Analytical Holographic Model,” [arXiv:2209.02074 [hep-th]].
- [75] T. Nishioka, “Entanglement entropy: holography and renormalization group,” *Rev. Mod. Phys.* **90** (2018) no.3, 035007 [arXiv:1801.10352 [hep-th]].
- [76] H. Casini and M. Huerta, “Entanglement and alpha entropies for a massive scalar field in two dimensions,” *J. Stat. Mech.* **0512**, P12012 (2005) [arXiv:cond-mat/0511014 [cond-mat]].
- [77] J. B. Hartle and S. W. Hawking, “Wave Function of the Universe,” *Phys. Rev. D* **28** (1983), 2960-2975.

- [78] J. Cotler, P. Hayden, G. Penington, G. Salton, B. Swingle and M. Walter,
“Entanglement Wedge Reconstruction via Universal Recovery Channels,” *Phys. Rev. X*
9, no.3, 031011 (2019) [arXiv:1704.05839 [hep-th]].